EPR of Exchange-Coupled Oligomers

BY DAVID COLLISON AND ERIC J.L. McINNES
School of Chemistry, The University of Manchester, Manchester M13 9PL, UK

1 Introduction

This review is an update of our previous SPR reviews on magnetically exchange-coupled oligomers,[1,2] and covers the literature in the two calendar years 2004 and 2005. As before we review the publications involving EPR spectroscopy of discrete molecular compounds containing more than one radical centre – polymeric materials are not covered. The discussion is largely restricted to compounds where 3 or more radical centres are present, but also include selected dimeric systems where we feel that these are of particular interest. The discussion is organised into coupled (i) *p*-block radicals, (ii) *d*-block radicals, (iii) mixed *p*/*d*-block radicals, (iv) mixed *d*/*f*-block radicals and (v) biological systems.

2 *p*-Block

This area is dominated by work on nitroxide species, driven by efforts towards fundamental understanding of magnetic exchange interactions in simple coupled $S = \frac{1}{2}$ systems and ultimately towards use as components in magnetic materials. We should note here that a major area and application of the study of interactions between nitroxide species is in distance measurements by PELDOR/DEER methods – in particular as applied to labelled biological systems – this is not covered in this review article.

Baumgarten and coworkers reported the pyrazolylbipyridine-bridged bis(nitronyl)nitroxide **1** and bis(iminonitroxide) **2**, and compare them to their terpyridine (terpy)-bridged analogues.[3] They describe these as ''multifunctional'' biradicals because of the potential metal chelating sites. For **1** and **2** the fluid toluene solution EPR spectra are characteristic of the strong exchange limit ($J \gg a_N$; J = isotropic exchange coupling constant, a_N = isotropic hyperfine interaction to ^{14}N) giving equally spaced 9- and 13-line spectra, respectively. Spin-triplet spectra are observed from frozen solutions (120 K),

Electron Paramagnetic Resonance, Volume 20

and simulation gives the axial zero-field splitting (ZFS) parameter $|D|$ as *ca.* 38 $\times 10^{-3}$ cm^{-1}. Fitting the temperature dependence of the intensity of the "half-field" $\Delta M_S = \pm 2$ transitions to the Bleaney-Bowers equation gives the singlet-triplet energy gaps ($2J$) as *ca.* 13 cm^{-1} (ferromagnetic) for **1** and $0.06 \leq 2|J| \leq 0.7$ cm^{-1} for **2**. These *J*-values are lower than those in the terpy analogues whilst the D-values are larger. This is consistent with the longer inter-radical distance in the terpy-bridged systems. The increase in *J* is concluded to be due to the two different spin polarisation pathways available in **1** and **2** due to the 5-membered heterocyclic rings in the bridges. Komaguchi *et al.* have investigated the efficiency of –($SiMe_2$)- based bridging for communication between two TEMPO radicals.[4] They studied the fluid solution EPR spectra of TEMPO-($SiMe_2$)$_n$-TEMPO (**3**) with $n = 1$ to 4. With $n = 1$ the strong exchange limit is observed, in contrast to single atom –C(=O)– or –S- links, from which the authors conclude that the Si atom enhances the through-bond exchange interaction. For $n = 4$ a monomer-like spectrum is observed (weak exchange limit). The spectra for $n = 3$ are temperature dependent, changing between (crudely) slow and rapid exchange on increasing temperature. They ascribe this to enhanced through-space intramolecular interactions due to the conformational freedom of the longer-chain links, and estimate activation barriers for this process (rotation about the Si–Si bonds) from variable-temperature line-shape analysis.

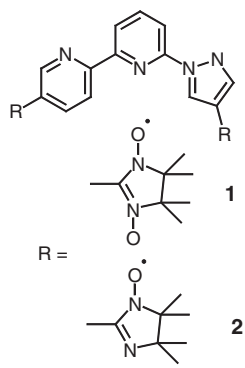

A very strong antiferromagnetic exchange interaction has been observed in the ethylene-bridged biradical **4**.[5] Spin triplet spectra are observed from **4** isolated in a polystyrene matrix, with $|D|/g\mu_B = 168$ G (μ_B = the electronic Bohr magneton), and the intensity as a function of temperature gives a singlet-triplet gap of 479 K. The authors note that analysis of *D* in a point-dipole approximation is not valid due to the strong exchange. Stroh *et al.* have shown that the exchange interaction between nitronyl nitroxides can be mediated by a diamagnetic Pt(II) fragment (complex **5** and its isomer with *meta*-substituted aryl linkers).[6] Strong exchange limit spectra are observed in fluid solution, although hyperfine coupling is not observed to ^{195}Pt or ^{31}P. There is a significant difference between the isotropic *g*-values for the *ortho*- and *meta*-substituted species (2.0094 and 2.0066, respectively) which the authors tentatively ascribe to different orbital overlap between the π-radical and metal *d*-orbitals.

The upper limit of $|J|$ is estimated as 1 cm^{-1}.

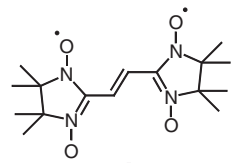

4

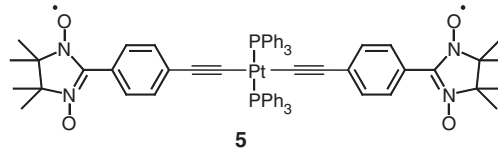

5

Takui *et al.* have continued their elegant studies of covalently bonded biradical-monoradical composites with the triradical **6**.[7] Here they synthesised strongly ferromagnetically coupled dimeric nitronyl-nitroxide fragments (via a *meta*-aryl linker, with exchange interaction J) which are then appended to a further nitronyl nitroxide via a σ-bound link which is expected to give rise to only weak exchange between the dimer and monomer (J', J''), thereby isolating $S = 1$ and $\frac{1}{2}$ species in the same molecule. By this route they hope to be able to produce "single component ferrimagnets" in the solid state. Solution EPR spectra in toluene reveal a 13-line spectrum due to hyperfine coupling to six ^{14}N nuclei, a_N (2.5 G) being about one-third of the splitting typically observed for monomeric nitronyl nitroxides indicating that both J and J' are significantly greater than a_N. However, on every third ^{14}N hyperfine line of this spectrum there is further coupling to ^{1}H, with a_H similar to that observed for a *m*-substituted benzoic acid derivative of the monoradical. The spectra can be analysed successfully by a perturbative approach confirming the result that $J \gg J'$, $J'' \gg a_N$. They conclude that the molecule can be described, in terms of magnetic behaviour, as independent $S = 1$ and $\frac{1}{2}$ moieties. Despite this, solid state samples of **6** do not show ferrimagnetic behaviour, due to only weak intermolecular coupling.

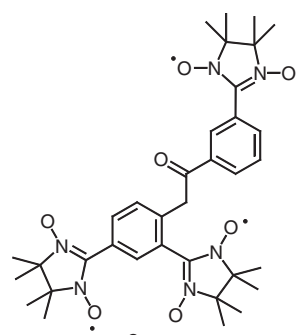

6

Turek and co-workers have extended their systematic study of phenylacetylene-, biphenyl- and *meta*-phenylene-bridged polyradicals to the tri- and tetra-radicals **7–9**.[8] The symmetrically substituted tri-radicals **7** and **8** were all found to have spin-quartet ground states from variable temperature EPR studies of frozen solutions, consistent with ferromagnetic coupling via the *m*-aryl and *m*-phenylacetylene or biphenyl pathways. The exchange interaction within the biradical moiety is found to be strongest for R = nitronyl nitroxide. The measured *D*-values for the quartet states (D_Q) were compared to those of the triplet states (D_T) for the corresponding *m*-aryl linked dimers (*i.e.* the diradical building blocks of the triradicals) through the relationship $D_Q = D_T/3$, valid if the dipolar interaction between the diradical and monoradical parts is insignificant. For the nitronyl nitroxide species there is good agreement, indicating that the coupling within the diradical part is not significantly perturbed by appending the monoradical moiety. However, for the imino nitroxide (and mixed nitronyl nitroxide-imino nitroxide) species there is significant disagreement which the authors interpret as being due to significant changes in the torsion angles of the radicals between the bi- and tri-radicals. In contrast to the tri-radicals, the tetra-radicals **9** are found to have singlet ground states, in defiance of the ''topological rules'' based on spin-polarisation ideas.

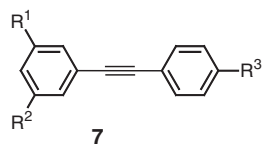

7

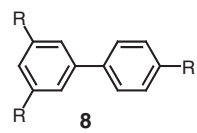

8

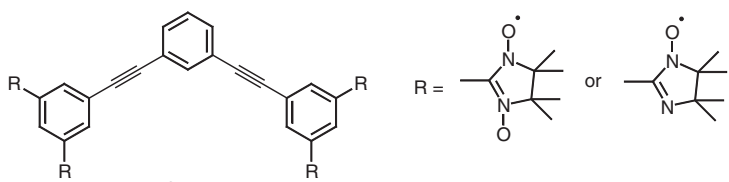

9

Veciana and co-workers have published two papers exploring the exchange between nitroxides in the substituted triphenyl phosphine oxides **10** and **11**.[9,10] In the di- and tri-nitronyl nitroxide substituted species **10** ($n = 2$, 3) the isotropic hyperfine interaction to ^{14}N is approximately one half and one third, respectively, of that seen for the monoradical $n = 1$. Coupling is seen to all nitrogens (strong exchange limit), and ^{1}H and ^{31}P coupling is also resolved for $n = 1$.[9] The spin density at P is found to increase with increasing *n*. They find a change in the sign of the spin density at P between the phosphine oxide and

analogous phosphine species (*i.e.* depending on whether the P has a lone pair of electrons or not) and speculate that this should have a significant effect on the sign of the exchange interaction. Unfortunately these proved to be too weak to measure by susceptibility methods. In order to address this they reported, in a second paper, the aminoxyl species **11** where the NO radical is conjugated directly into the aryl rings.[10] Coupling to three equivalent ^{14}N, six ^{1}H and one ^{31}P is observed in the fluid EPR spectrum (strong-exchange limit). Although they expected this species to be ferromagnetically coupled based on spin-polarisation arguments, it turns out to be antiferromagnetically coupled with $J = -7.55$ cm^{-1} and the authors conclude there must be another mechanism. The frozen solution EPR spectrum at 5 K is that of an isolated $S = \frac{1}{2}$ species. An antiferromagnetically coupled equilateral triangle would be expected to lead to a degenerate pair of $S = \frac{1}{2}$ states (spin frustration), thus the EPR behaviour suggests distortion to an isosceles triangle.

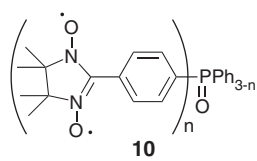

10

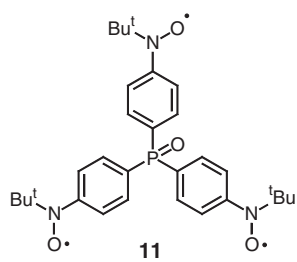

11

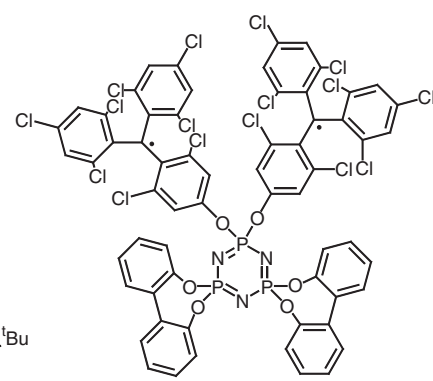

12

Carriedo *et al.* have also studied exchange interactions, mediated by phosphorus, in the disubstituted triphosphazine derivative **12**.[11] Fluid-solution EPR of **12** shows hyperfine coupling to a single ^{31}P (consistent with exchange via the –O–P–O– fragment) and to twelve ^{1}H's. The a_H coupling is half that observed for the monoradical analogue hence $J \gg a_H$. The resolution in further tri- and tetra-substituted analogues is much poorer, consistent with much smaller hyperfine interactions, as expected in the strong exchange limit, but that can be extracted by simulation. These show ^{31}P coupling to two nuclei, hence there is electronic communication via the P-N-P backbone of the phosphazine ring. Finally, Rajca *et al.* have prepared the diradical **13**, an analogue of trimethylenemethane (TMM), prepared by oxidation of its tetra-anion in THF.[12] EPR studies show that there is a strong ferromagnetic coupling

between the radical centres, with a triplet-singlet gap of at least 100 K and a value in the triplet state of $D = 0.004$ cm^{-1}, smaller than that observed in TMM.

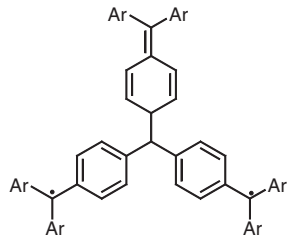

13

3 *d*-Block

Elsenbroich and co-workers have published a beautiful series of papers on electronic communication in the trovocenyl-based polyradicals {trovocene, TVC = [(η^7-C_7H_7)V(η^5-C_5H_5)]}.[13–16] In a series of dimers where the TVCs are linked by acetylides via the cyclopentadienyl (Cp) moieties [(C_7H_7)V(C_5H_4-R-C_5H_4)V(C_7H_7)],[13] biradical-like spectra are observed in fluid solution with 15-line patterns due to the two equivalent ^{51}V nuclei, but with intensities that deviate from the binomial pattern expected in the strong exchange limit. This allows the *J*-values to be determined by spectrum simulation, giving (antiferromagnetic) $J = -0.92$ [R = –(C≡C)-bridge], -0.56 [R = –$(C{\equiv}C)_2$–] and -0.005 cm^{-1} [R = *p*-$(C{\equiv}C)_2$–C_6H_4], compared to the "parent", directly linked, ditrovocenyl which has $J = -2.8$ cm^{-1}. They conclude from the systematic attenuation of *J* with increasing *n* (0–2) that it should be possible to detect exchange up to $n = 15$ by EPR. The *J*-values are weak because the V $3d_{z^2}$ magnetic orbitals are orthogonal to the molecular orbitals of the Cp ligands with little spin density on the bridging ligands. In a second paper they study further ditrovocenyls where R = –CH_2–, –CH_2CH_2–, –C(=CH_2)–, and *cis* and *trans* –C(Me)=C(Me)–.[14] The strong exchange limit is only observed with R = –CH_2–. They argue that in this species the single sp^3 carbon forces tilting of the two Cp rings towards each other, facilitating exchange via overlap of the π-systems. The next strongest interaction is observed for the sp^2 bridged R = –C(=CH_2)–. There is an order of magnitude difference in *J* between the two isomeric ethylene bridged species, in favour of the *trans* isomer. The authors argue that this is because the Cp rings can lie co-planar in the *trans* isomer. Surprisingly a significant *J*-value is observed for R = –CH_2CH_2– which must either be due to a σ-spin polarisation mechanism or through hyperconjugation of the C–H bonds in the Cp rings. The same group have extended this work to a tetra-trovocenyl radical, [1,2,4,5-(C_7H_7)V(C_5H_4)]$_4$(C_6H_2).[15] 29 lines are

observed in the fluid solution EPR spectrum with a_V *ca.* one quarter of that for trovocenyl itself. Hence, this approaches the strong exchange limit, although the three different exchange pathways precluded determination of the *J*-values. Finally, these authors have probed the effect of a diamagnetic *metal* fragment as a linker between derivatised vanadocenes, in the complexes [{$(Me_2P\text{-}C_6H_5)_2V$}$_2$Ni] and [{$(Me_2P\text{-}C_6H_5)_2V$}$_2$CoH].[16] The V...V exchange is found to be similar between the two complexes, *ca.* 0.3 cm^{-1}, and there is no resolution of ^{59}Co hyperfine in the latter, so there is little effect on the exchange.

A further example of biradical-like spectra from transition metal ions is given by Wong *et al.*[17] for the di-copper(II) macrocycle **14**. Fluid-solution EPR gives an intermediate exchange-type spectrum ($J \approx a_{Cu}$). However, on formation of a [2]catenane with the di-gold(III) analogue (a dication), the exchange is "switched off" or, alternatively, the two Cu(II) ions are insulated from one another by the diamagnetic, non-covalently bound, Au(III) ring. The EPR spectrum of the catenane species is indistinguishable from that of a monomeric Cu(II) *bis*-dithiocarbamate complex.

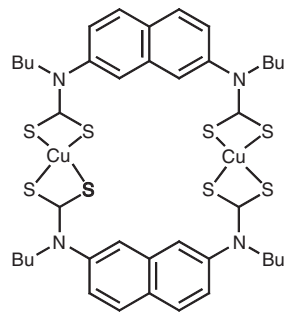

14

Bond *et al.* have published EPR studies of the Cu(II) dimers $[Cu_2(CN)L]^{3+}$, where L is an aza-cryptand (for example, ligand **15**).[18] The Cu(II) ions have trigonal bipyramidal coordination geometry with the unique axis along the Cu...Cu vector bridged by CN^-. The Cu(II) ions are antiferromagnetically coupled but, unusually for Cu dimers, have d_{z^2} ground states as confirmed by the EPR spectra of the $S = 1$ excited states which have $g_{x,y} > g_z \approx g_e$ with g_z collinear with the principal axis of the ZFS tensor.

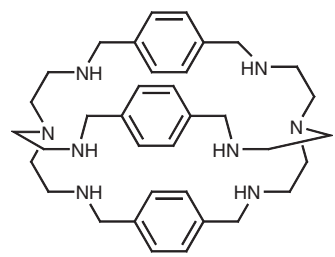

15

Yano *et al.* have reported a low-temperature single-crystal X- and Q-band study of the mixed-valence Mn(III)Mn(IV) dimer $[Mn_2O_2(phen)_4](PF_6)_3$,[19] showing unusually well-resolved spectra for an undiluted crystal, with good resolution of the ^{55}Mn hyperfine splittings. At 9 K only the $S = \frac{1}{2}$ ground state of this antiferromagnetically coupled dimer is populated. The data are analysed with an effective $S = \frac{1}{2}$ spin Hamiltonian. Near axial g-values are found with the "unique" lowest g-value (g_z) perpendicular to the Mn_2O_2 core. The hyperfine couplings to Mn(III) and Mn(IV) are determined and, as expected, those for Mn(III) are significantly anisotropic (with the "unique" A_z axis co-parallel with g_z) while those for Mn(IV) are nearer isotropic. These data are rationalised in terms of a vector-coupling model based on data for Mn(III) and Mn(IV) ions doped in rutile. The authors discuss the relevance of their results for biological systems such as photosystem II, highlighting that the oft-quoted "$2A_{Mn(IV)} = A_{Mn(III)}$" relationship used to interpret multi-line mixed-valence manganese spectra is not valid when the anisotropy of the hyperfine interaction is taken into account.

A series of papers from several groups deals with antiferromagnetically coupled triangles of $S = \frac{1}{2}$ paramagnets.[20–23] Such species are of interest because for an equilateral triangle an orbitally degenerate ground state should result (a pair of degenerate $S = \frac{1}{2}$). This is the strict definition of "spin frustration"[24] although many authors use this term simply to mean competing antiferromagnetic interactions. Such systems can relieve the orbital degeneracy via spontaneous distortion to isosceles or lower symmetry (energy gap δ, a magnetic Jahn-Teller distortion) or via antisymmetric exchange interactions (G), giving rise to a total zero-field splitting (Δ) between the two $S = \frac{1}{2}$ states of $\Delta^2 = \delta^2 + 3G^2$. Liu *et al.* report such interactions in $[Cu_3X(Hpz)_2(\mu_2\text{-}pz)_3(\mu_3\text{-}OMe)]X$ [X = Cl^-, Br^-; Hpz=3{5}-(mesityl)pyrazole] where the three Cu(II) ions are in a (near) isosceles triangle bridged by a central μ_3-OMe.[20] Powder Q-band EPR at 4 K reveal two strong transitions at effective g-values of $g_{eff} = 2.21$ and 1.47 (X = Cl^-) and 2.19 and 1.52 (X = Br^-). In an axial system subject to antisymmetric exchange EPR transitions are expected at the true $g_\parallel$ and at $g_\perp{}'$ which is related to the true $g_\perp$ by $g_\perp{}' = g_\perp[\{\delta^2\text{-}(h\nu)^2\}/\{\Delta^2\text{-}(h\nu)^2\}]^{1/2}$ which simplifies to $g_\perp{}'/g_\perp \approx \delta/\Delta$ if $h\nu \ll \Delta,\delta$ and this can be used to estimate the contribution of the lower than trigonal symmetry to the total ZFS Δ. The authors note that in order to see $g_\perp{}' \ll g_e$ (and hence the true $g_\perp$) antisymmetric exchange effects must be in action (*i.e.* $\delta \neq \Delta$), and these are estimated from powder magnetic susceptibility data in conjunction with the EPR spectra. In this work the molecule has lower than trigonal symmetry anyway. Ideally such effects would be studied in single crystals of a crystallographically trigonally-symmetric trimer, and this is the subject of a much more detailed study by Solomon and co-workers on the D_3 (crystal structure determined at −130°C) symmetry $[Cu_3(DBED)_3(\mu_3\text{-}OH)](ClO_4)_3$ (DBED = N,N′-di-^{t}Bu-ethylenediamine).[21] Here the (antiferromagnetic) isotropic J is $-105\ cm^{-1}$. Powder EPR spectra at 5 K show a single broad resonance at $g_{eff} = 2.32$ with a partially resolved four-line hyperfine pattern with $A_\parallel = 74 \times 10^{-4}\ cm^{-1}$. X-band single crystal studies at 3.7 K show a remarkable orientation dependence: with the

applied field (H) parallel to the 3-fold axis of the molecule (z, $\theta = 0^\circ$) a spectrum is observed similar to that from the powder; when H is rotated away from z this broadens and shifts up-field rapidly, reaching $g_{\text{eff}} \approx 1.2$ before being unobservable beyond $\theta = 60^\circ$. The total ZFS Δ is determined from magnetic circular dichroism (MCD) studies as 67 cm^{-1}. These data are analysed via the spin Hamiltonian:

$$\begin{aligned}\hat{H} = &-2J(\hat{S}_1.\hat{S}_2 + \hat{S}_2.\hat{S}_3 + \hat{S}_1.\hat{S}_3) + \delta(S_1.S_2) \\ &+ \delta(S_1.S_3) + \mathbf{G}\left(\left[\hat{S}_1 \times \hat{S}_2\right] + \left[\hat{S}_2 \times \hat{S}_3\right] + \left[\hat{S}_3 \times \hat{S}_1\right]\right) \\ &+ (g_z \cos\theta + g_{xy} \sin\theta)\beta H(\hat{S}_1 + \hat{S}_2 + \hat{S}_3)\end{aligned}$$

where **G** is the antisymmetric exchange vector. When $\theta \neq 0^\circ$, the two $S = \frac{1}{2}$ states mix giving a non-linear dependence on H and low g_{eff}. Transitions within the lower doublet should only be observed when $\delta \neq 0$ and hence the EPR provides direct evidence for a spontaneous symmetry lowering from D_3, and fitting the angular dependence of the EPR gives $\delta = 17.5$ cm^{-1} which in turn gives $G = 36$ cm^{-1}. The authors point out that the origin of the antisymmetric exchange is in efficient ground state-excited state exchange interactions between the Cu(II) ions. The same group followed this work with a study of a ferromagnetically coupled, trigonally (C_3) symmetric Cu(II) trimer, [Cu_3(**16**)(μ_3-O)](ClO_4)$_4$.[22] There is a rather large ZFS in the spin-quartet ground state ($D = -2.5$ cm^{-1}), determined from the temperature dependence of the intensity of the solid state EPR spectrum ($g_{\text{eff}} = 3.64$ and 2.06 at X-band).

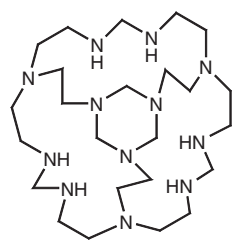

16

The authors discuss the origin of this large splitting in terms of the anisotropic exchange which they point out has the same physical basis as the antisymmetric exchange – coupling between the ground state of one metal ion [in this case d_{z^2} because of the trigonal bipyramidal geometry at each Cu(II) ion] and the excited state of another. Glaser *et al.* report another ferromagnetically coupled Cu(II) trimer, [Cu_3(talen)], where talen is a tris-salen derived ligand.[25] Well-resolved perpendicular and parallel mode X-band spectra are observed from frozen solutions at 3 K. Although D is too small to resolve fine structure, modelling the relative intensities of the allowed and forbidden (half-field) transitions gave $|D| = 74 \times 10^{-4}$ cm^{-1}. The spectra show 10-line hyperfine patterns due to the three equivalent Cu(II) ions, which they claim is the first time this has been observed. Nellutla *et al.* used EPR to prove the localisation of the spin ground state on a single copper ion in the penta-copper

$[Cu_5(OH)_4(H_2O)_2(A\text{-}\alpha\text{-}SiW_9O_{33})_2]^{10-}$ where the Cu(II) ions essentially define a rectangular based pyramid with the apical Cu(II) equally bound to the other four.[26] This cluster is sandwiched between the diamagnetic polyoxotungstates. Low-temperature EPR gives a rhombic $S = \frac{1}{2}$ spectrum with hyperfine to a single Cu(II) ion which they interpret, in conjunction with magnetic susceptibility data, as a well isolated $S = \frac{1}{2}$ ground state located on the apical Cu(II) ion. Halcrow and co-workers report a heptametallic Cu(II) cluster $[\{Cu_3(Hpz)_6(\mu_3\text{-}Cl)(\mu_3\text{-}OH)_3\}_2Cu]$ based on two vertex-sharing $\{Cu_4O_4\}$ heterocubanes.[27] From modelling magnetic susceptibility data the $S = \frac{1}{2}$ ground state arises largely from the linear Cu_3 fragment in this topology. Q-band EPR of a powder at 4 K reveals an axial $S = \frac{1}{2}$ spectrum with a well-resolved eight-line hyperfine pattern on the parallel feature. This can be simulated by assuming hyperfine coupling to two equivalent and one inequivalent Cu nuclei with a 2.5:1 ratio of magnitudes. Significantly above or below this ratio gives simpler five or seven-line patterns, respectively, towards the expected limits for coupling to two or three equivalent Cu. The three copper ions have similar coordination environments, and the difference in the coupling to the central Cu ion is rationalised from a simple vector coupling analysis assuming the $|S_{13},S_{total}> = |1,1/2>$ ground state of a linear trimer.

Three papers have appeared detailing EPR studies on "molecular wheel" complexes. Pilawa *et al.* studied the antiferromagnetically coupled $[Fe_6(tea)_6]$ (tea = trianion of triethanolamine) where the six Fe(III) ions are bridged by the alkoxide arms of the ligand.[28] The antiferromagnetic coupling leads to a diamagnetic ground state but EPR transitions are observed from the first $S = 1$, 2, 3 and 4 excited states in an X-band single crystal study at 30 K. The spectra had previously been analysed by a full interaction Hamiltonian to obtain the single-ion and exchange parameters: in this work the authors probed relaxation dynamics via the linewidths. Below *ca.* 30 K the linewidths are dominated by inter-cluster dipolar interactions and in order to model this it is necessary to consider states up to $S = 4$, while above this temperature spin-lattice relaxation dominates. The odd-membered ring $[(C_6H_{11})_2NH_2][Cr_8NiF_9(O_2CCMe_3)_{18}]$ has been studied by Sessoli and co-workers.[29] Here the antiferromagnetic coupling gives rise to an $S = 0$ ground state, but the odd number of metal ions means that a simple "up-down" arrangement of spins cannot be satisfied around the ring – a form of frustration – and the authors make the analogy to a Möbius strip. The first excited state is $S = 1$ but the nature of this state is different depending on the relative magnitude of the Cr…Cr and Cr…Ni exchange interactions. The g-value of the $S = 1$ state is expected to be approximately equal to g_{Ni} [single-ion g-value of the Ni(II) ion] if $J_{CrCr} \gg J_{CrNi}$ from consideration of the form of the wavefunction by a simple vector coupling model. If $J_{CrCr} \ll J_{CrNi}$ then a similar analysis predicts $g = 3/2g_{Cr}\text{-}1/2g_{Ni}$. Because the g_{Cr} and g_{Ni} are expected to be substantially different this allows determination of the relative amplitude of the exchange interaction from the EPR spectrum of the $S = 1$ excited state. Low temperature powder spectra at 285 GHz suggest that $J_{CrCr} \ll J_{CrNi}$. A ferromagnetically coupled decametallic Cr(III) ring, $[Cr_{10}(OMe)_{20}(O_2CCMe_3)_{10}]$, has been studied by Sharmin *et al.*[30] Although magnetic susceptibility measurements

show that the average *J*-value is ferromagnetic, the low-temperature EPR spectra measured between 50 and 70 GHz on powder and single crystal samples are more consistent with an $S = 9$ ground state ($D/k_B = -0.045$ K, where k_B is the Boltzmann constant). This can only result if some of the Cr. . .Cr interactions are antiferromagnetic, which is consistent with the molecular symmetry – there are in principle five different *J*-values given the two-fold symmetry of the molecule.

Clusters with such high-spin ground states are of interest because this can lead to unusual low-temperature physics: for example, when combined with a significant negative ZFS this can lead to a barrier to relaxation of magnetisation and hence a molecular magnetic memory effect. Such materials have become known as "single molecule magnets" (SMMs). One of the smallest SMMs prepared to date is the heterodimetallic $[Mn^{III}Cu^{II}(5\text{-Br-sap})_2(MeOH)]$ (5-Br-sap = 5-bromo-2-salicylideneamino-1-propanol) reported by Oshio *et al.*[31] The two metal ions are strongly coupled ferromagnetically via two alkoxide arms of the ligand to give a well isolated $S = 5/2$ ground state. Well-resolved 342 GHz EPR spectra are consistent with this and give $D = -1.81$ cm^{-1}. This cluster *D* is then simply related to the single ion Mn(III) ZFS via $D_{5/2} = (16/25)D_{Mn}$, although this analysis neglects dipolar contributions.

One of the important magnetic phenomena observed in SMMs is quantum tunnelling of magnetisation (QTM) – this can occur between pairs of M_S states on either side of the energy barrier to relaxation, *e.g.* in a spin *S* with negative *D* it can be possible for the system to tunnel between $M_S = -S$ to $+S$ in zero field where these states are degenerate. This can often be observed as a step in magnetisation *vs* applied magnetic field loops. An unusually large step is observed in such a measurement for the $S = 4$ ground state SMM $[Ni(hmp)(^tBuEtOH)Cl]_4$ (hmp = anion of hydroxymethylpyridine; ^{t}BuEtOH = 3,3-dimethyl-1-butanol) implying very fast QTM at zero field.[32,33] This molecule has axial (S_4) symmetry, hence rhombic *E* terms in the spin Hamiltonian are forbidden. Single crystal measurements with the applied field varied in the hard plane of magnetisation (xy) reveal a four-fold periodicity. These can be reproduced using a Hamiltonian including a fourth order term $B_4^4(\hat{S}_+^4 - \hat{S}_-^4)$ which induces mixing between states differing between $M_S \pm 4$. Simulation gives $B_4^4 = 4 \times 10^{-4}$ cm^{-1} which equates to a large 10 MHz tunnel splitting between the $M_S \pm 4$ states in zero field. Cornia and co-workers have observed important symmetry effects on the barrier height in a family of tetrametallic SMMs based on centred triangles of Fe(III).[34,35] Antiferromagnetic coupling leads to an $S = 5$ ground state. The parent molecule $[Fe_4(OMe)_6(dpm)_6]$ (Hdpm = dipivaloylmethane) has only C_2 point symmetry and EPR studies reveal a ground state ZFS of $D/k_B = -0.29$ K. The six methoxides can be replaced with the tripodal tris-alkoxide ligands $RC(CH_2O^-)_3$ (R = Me or Ph). When R = Ph C_2 is maintained, but with R = Me higher symmetry (D_3) is imposed. For both derivatives the ground states have much higher D/k_B (−0.64 and −0.61 K, respectively, determined by 230 GHz EPR measured on powders between 30 and 10 K) leading to much larger magnetisation blocking temperatures. The authors speculate that this may be due to different extents of trigonal distortion

of the apical iron sites in the different molecules and hence differing single-ion ZFS.

Christou's group report a further example of the importance of molecular symmetry on the magnetic behaviour of clusters.[36] The tetrametallic $Mn(III)_3Mn(IV)$ cluster $[Mn_4O_3(O_2CPh)_4(dbm)_3]$ has an $S = 9/2$ ground state, and is part of a family of $\{Mn_4O_3X\}$ heterocubane structures studied by this group. When $X = Cl^-$ the cluster has pseudo-C_3 symmetry. Here X is an η^2,μ_3-carboxylate which opens up one edge of the heterocubane reducing the symmetry to pseudo-C_S. This leads to a better alignment of the Mn(III) Jahn-Teller axes with each other than in the parent $X = Cl^-$ cluster (where they intersect at X). 249 GHz EPR studies on a single crystal gives $D = -0.646$, $E = 0.14$ cm^{-1}, both significantly larger than those observed for $X = Cl^-$ ($D = -0.53$ cm^{-1}, $E = 0$). Despite the larger $|D|$ value the lower symmetry molecule shows faster magnetisation relaxation rates, and this is ascribed to the non-zero E which leads to rapid QTM in zero applied field.

van Slageren *et al.* have reviewed the application of frequency-swept EPR to SMMs and related species,[37] pointing out that it has the advantage for measuring ZFS parameters of being measured in zero applied field! A nice example of the application of this technique is on Brechin and co-workers' $S = 17/2$ ground state $[Mn_9O_7(O_2CMe)_{11}(thme)(py)_3(H_2O)_2]$ {H_3thme = tris(hydroxymethyl)ethane}, the core of which contains a trigonal $\{Mn(IV)_3(\mu_3\text{-}O)\{Mn(III)_4Mn(II)_2O_6\}$ ring.[38] Frequency-swept EPR spectra in zero applied magnetic field, measured on a powder between 10 and 2 K and in the frequency range 2.8–5.0 cm^{-1}, show three resonances at 3.79, 3.41 and 2.95 cm^{-1}. The highest frequency transition is the most intense, and increases in intensity with decreasing temperature, showing that D is negative – this is the $M_S = \pm 17/2$ to $\pm 15/2$ transition. Fitting to these data gives $D = -0.247$ cm^{-1}, $E = 0$, $B_4^0 = +4.6 \times 10^{-4}$ cm^{-1} where the fourth-order operator is:

$$\hat{O}_4^0 = 35\hat{S}_z^2 - [30S(S+1) - 25]\hat{S}_z^2 - 6S(S+1) + 3S^2(S+1)^2$$

Kirchner *et al.* studied the lineshapes of the transitions in this complex, and in the anionic $(PPh_4)[Mn_{12}O_{12}(O_2CEt)_{16}(H_2O)_4]$ (the one-electron reduction product of the parent class of SMMs, see later) which has an $S = 19/2$ ground state.[39] In the former the lineshapes are Gaussian and temperature independent, *i.e.* the resonances are inhomogeneously broadened, and this is likely due to D-strain effects. In contrast, those of $(PPh_4)[Mn_{12}O_{12}(O_2CEt)_{16}(H_2O)_4]$ are Lorentzian and temperature dependent – they are homogeneously broadened. The authors relate this to the lifetimes of the excited-state M_S levels, estimating lifetimes of 50–58 ps from the $M_S = \pm 19/2$ to $\pm 17/2$ transition depending on temperature. This observation of homogeneous broadening is unusual for a SMM, and stands in contrast to work by the same group on the archetypal SMM, $[Mn_{12}O_{12}(O_2CMe)_{16}(H_2O)_4]\cdot 2(MeCO_2H)\cdot 4H_2O$ ("Mn12Ac"; $S = 10$ ground state), where inhomogeneously broadened Gaussian lines are observed. The cause of this difference between Mn12Ac and $(PPh_4)[Mn_{12}O_{12}(O_2CEt)_{16}(H_2O)_4]$ is

unclear. Vongtragool *et al.* have also used the frequency-swept EPR experiment to measure the relaxation of Mn12Ac as follows:[40,41] the molecule is cooled in an applied field, thus magnetising the system, and only the $M_S = -10$ to -9 transition is observed at a higher frequency *cf.* zero-field measurements. Now the applied field is reversed and a new peak ($M_S = +10$ to $+9$) is observed to grow in down-frequency (*cf.* the zero-field experiment) as the molecule slowly depopulates from the meta-stable $M_S = -10$ to the new ground state of $M_S = +10$. Monitoring evolution of the intensities with time gives a relaxation time of *ca.* 150 minutes for an applied field of 0.45 T.

The literature on EPR studies of SMMs is still dominated by Mn12Ac and its ever-increasing number of derivatives. In addition to the above studies, several reports have appeared from Hill and co-workers highlighting the importance of crystal disorder in determining observed magnetic properties. Although Mn12Ac crystallises in a tetragonal space group and has global 4-fold symmetry, Cornia *et al.* had previously shown that disorder of the solvents of crystallisation leads to a symmetry-breaking effect leading to six different isomers in the lattice, only two of which retain four-fold symmetry.[42] Hill provided evidence for this from detailed single-crystal studies with the applied field oriented in the hard plane of magnetisation (and narrow ranges of angles deviating from this plane).[43] They demonstrate that the observed four-fold periodicity in this plane and the presence of anomalous peaks (peaks not expected from a simple model assuming a single magnetically unique molecule) can be modelled by assuming (i) local distortions from four-fold symmetry (introducing non-zero E) in subsets of molecules as described by Cornia, and (ii) tilting of the easy axis of magnetisation (molecular z axes) of subsets of molecules away from the unique crystal axis. This latter effect introduces subsets of molecules with transverse field components when a magnetic field is applied along the *crystal's* easy axis of magnetisation, and the authors speculate that this could be the mechanism for QTM transitions between M_S states differing by odd integer values. These have been observed in magnetisation *vs.* applied field studies, but cannot be accounted for by non-zero E (which mixes states differing by $M_S \pm 2$) or B_4^4 ($M_S \pm 4$). Christou and co-workers have prepared new variants of Mn12 in order to try to remove the solvent disorder problem.[44,45] The extra structure observed in the high frequency EPR spectra of Mn12Ac (see above) is absent in those of $[Mn_{12}O_{12}(O_2CCH_2Br)_{16}(H_2O)_4]\cdot 4CH_2Cl_2$ and $[Mn_{12}O_{12}(O_2CCH_2Bu^t)_{16}(H_2O)_4]\cdot MeOH$ which both have crystallographic S_4 symmetry (as does Mn12Ac, notwithstanding solvate disorder), thus implying that these may have true fourfold *molecular* symmetry without disorder and that there is no tilting of the molecules' easy axis of magnetisation with respect to each other. In contrast to Mn12Ac, the solvate molecules in these two materials do not hydrogen-bond to the cluster. Hill also reports evidence for a low-lying $S = 9$ excited state in $[Mn_{12}O_{12}(O_2CCH_2Br)_{16}(H_2O)_4]\cdot 4CH_2Cl_2$ from variable temperature single crystal EPR studies at 60–80 GHz.[46] With the applied magnetic field perpendicular to the easy axis of magnetisation, weak extra peaks are observed between those assignable to the $S = 10$ ground state. From the variable temperature behaviour – these peaks reach a maximum in intensity at *ca.* 20 K – they

conclude these are due to an $S = 9$ excited state with otherwise similar spin Hamiltonian parameters to the $S = 10$ ground state. They place the $M_S = \pm 9$ states of the $S = 9$ at *ca.* 40 K above the $M_S = \pm 10$ states of the $S = 10$, which means that the two S manifolds overlap considerably. EPR studies of two other Mn12 variants have been reported. Hendrickson gives another example of a "Jahn-Teller isomer", in $[Mn_{12}O_{12}(O_2CC_6H_4\text{-p-Me})_{16}(H_2O)_4]\cdot CH_2Cl_2$.[47] The Mn12 family contain eight Mn(III) ions and four Mn(IV) ions and in Mn12Ac itself the Jahn-Teller distortion axes of the high spin d^4 Mn(III) ions are co-parallel with each other and with the molecular z axis (easy axis of magnetisation). It is this that gives rise to the large, negative cluster ZFS. However, in some Mn12 variants one or more of the Jahn-Teller axes are tilted with respect to the rest, and $[Mn_{12}O_{12}(O_2CC_6H_4\text{-p-Me})_{16}(H_2O)_4]\cdot CH_2Cl_2$ is an example of this. Curiously 324 GHz EPR gives $D = -0.47$ cm^{-1} which is similar to that reported for Mn12Ac itself. Hachisuka *et al.* report a $Mn_{11}Cr$ cluster where one Mn(III) ion in Mn12Ac has been replaced by Cr(III) giving rise to a $S = 19/2$ ground state.[48] Surprisingly they find the other ground state spin Hamiltonian parameters to be identical to those of Mn12Ac – replacement of an anisotropic Mn(III) ion with a pseudo-isotropic Cr(III) ion had little influence on the cluster anisotropy.[48]

Finally, in addition to the frequency-swept EPR studies reviewed above, there are two interesting "new" experimental procedures reported for high spin ground state clusters. Piligkos *et al.* have performed a single crystal parallel mode X-band EPR study of the $S = 6$ ground state $[Cr_{12}O_9(OH)_3(O_2CCMe_3)_{15}]$.[49] Although widely exploited in the study of high spin FeS clusters in biological systems, this is the first application of parallel mode modulation to very high spin molecular clusters. The authors discuss the consequences of the different selection rules ($\Delta M_S = 0$ *cf.* ± 1) for selective connection of pairs of eigenstates in high spin clusters. Two groups report the use of magnetisation-detected EPR as illustrated on the $S = 10$ ground state SMM $[Fe_8O_2(OH)_2(OH)_{12}(tacn)_6]Br_8$ ("Fe8"; tacn = 1,3,5-triazacyclononane).[50–53] Petukhov *et al.* monitor the magnetisation response of a single crystal of Fe8 under microwave radiation (pulsed or c.w.) as the applied magnetic field is swept, using a Hall-probe magnetometer (an array of 10×10 μm^2 Hall bars).[50] The sensitivity of the Hall-probe technique allows measurements on micron-sized single crystals. Data are measured at 118 GHz and between 2 to 20 K. The authors also illustrate that the spectra can be transformed to determine the spin temperature of the sample by mapping onto variable temperature magnetisation *vs.* field curves (in the absence of microwave radiation). Cage *et al.* report a conceptually similar experiment but using a commercial SQUID magnetometer where the Fe8 single crystal (*ca.* 3 mm^3) is under irradiation at 95 or 141 GHz.[51,52]

4 Mixed *p*/*d*-Block Radicals

Wieghardt and co-workers have continued their systematic studies of coordination complexes of redox non-innocent ligands. The *o*-diiminobenzosemiquinonate

radical anion ligand (**17**) complexes to Fe(III) with a co-ligand X to form five-coordinate species $[Fe(\mathbf{17})_2X]^{n+}$ where $X = I^-$ ($n = 0$) or PBu_3 ($n = 1$).[53] X-band EPR spectra at 10 K in frozen solutions reveal $S = \frac{1}{2}$ spectra, consistent with this ground state as shown by magnetic susceptibility data. Both species have rhombic *g*-values with all *g*-values greater than g_e and this is inconsistent with a simple assignment as low spin Fe(III) with two diamagnetic ligands as had been previously suggested. However, this *is* consistent with two radical ligands coordinated to an intermediate spin $S = 3/2$ Fe(III) ion and this is supported by Mössbauer spectra. The $S = \frac{1}{2}$ ground state arises from strong antiferromagnetic coupling between the metal ion and the radical ligands, where the inter-ligand exchange is negligible. Interestingly, when $X = I^-$ a well-resolved hyperfine pattern due to the ^{127}I nucleus is observed that can be simulated with inclusion of the ^{127}I hyperfine (**A**) and electric quadrupole (**P**) interactions. They further note that the spectra can only be reproduced by including non-coincidence between the **A** and **P** principal axes.

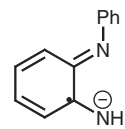

17

The relatively rare intermediate spin state for iron(III) is also invoked in the *bis*-(benzene-1,2-dithiolato) complexes $[Fe_2(\mathbf{18})_3(\mathbf{18}\cdot)]^-$ and $[Fe(\mathbf{18}\cdot)_2(PMe_3)]^+$.[54] The X-band spectrum of the dimetallic species at 10 K shows a near-axial spectrum with low *g*-anisotropy (g_1–$g_3 = 0.05$), only consistent with an *S*-centred radical. This is consistent with the magnetic model where the antiferromagnetic exchange between the two Fe(III) ions is much stronger than that between the metal ions and the radical ligand. In the monometallic species a rhombic $S = \frac{1}{2}$ is observed at 10 K in frozen solution, with much larger *g*-anisotropy (g_1–$g_3 = 0.15$). In contrast to the cationic $[Fe(\mathbf{18}\cdot)_2(PMe_3)]^+$, the reduced, anionic $[Fe(\mathbf{18})_2(PMe_3)]^-$ exhibits effective *g*-values typical of an $S = 3/2$ state with large *D*, consistent with the ligands being in their reduced, dianionic and diamagnetic form. While EPR is obviously useful in characterisation of the redox states of ligand and metal, the authors conclude that the best ''fingerprints'' for oxidation state of both metal and benzene-1,2-ditholate ligands in such complexes come from infrared (IR), visible/near-IR and Mössbauer spectroscopies.

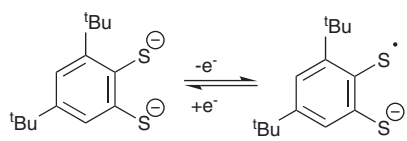

18 **18·**

Thomas *et al*. have probed the electronic structure of copper(II) complexes of the *bis*-salen type ligand **19**, [Cu(**19**)], as a possible model for galactose

oxidase.[55] The complex undergoes two one-electron oxidations which are assigned as oxidations of the ligand to phenoxyl radicals by comparison with the redox behaviour of the free ligands. [Cu(**19**)] has a normal tetragonal Cu(II) EPR spectrum, while the monocation $[Cu(\mathbf{19})]^{+}$ is found to be EPR silent at X-band and 4–100 K. The dication $[Cu(\mathbf{19})]^{2+}$ has resonances at $g_{eff} = 8.0, 4.7, 2.9$ and 1.5 which the authors state belong to the $M_S = \pm 1/2$ (4.7, 2.9) and $\pm 3/2$ (8.0, 1.5) doublets of a zero-field split $S = 3/2$ state resulting from ferromagnetic coupling of the π-radical ligands with the Cu(II) ion. The interesting hetero-three-spin system **20** is reported by Kirk *et al.*[56] The X-band EPR spectrum of **20** in frozen solution at 5 K gives effective *g*-values typical of an $S = 3/2$ state with large $|D|$, implying ferromagnetic coupling of the three components; simulation gives $|D| = 0.5\ cm^{-1}$. The authors attempt to rationalise the strong ferromagnetic coupling between the two organic radical centres in a valence-bond configuration-interaction model.

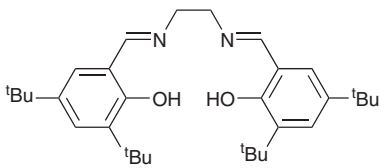

19

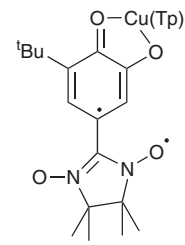

20

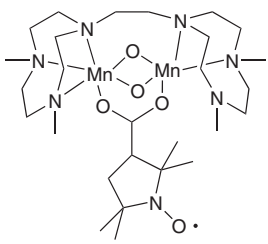

21

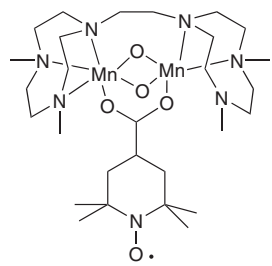

22

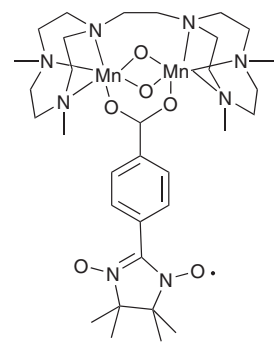

23

Finally, Bill, Wieghardt and co-workers have published a detailed multi-frequency (S, X, Q-band) EPR study of heterovalent Mn(III)Mn(IV) dimers coupled to nitroxide free radicals (**21–23**),[57] with relevance to biological systems such as the tyrosine radical – manganese cluster in photosystem II. The Mn(III)Mn(IV) dimers are strongly antiferromagnetically coupled ($J \approx -130\ cm^{-1}$) to give well isolated $S = \frac{1}{2}$ ground states and these couple weakly (J') with the appended free radical. Studies on the isolated Mn(III)Mn(IV) dimers (no free radical) and Mn(IV)Mn(IV)-appended radical systems define the magnetic

parameters of the isolated fragments. The large J and weak J' mean that the low temperature EPR spectra are dominated by the singlet-triplet system arising from the coupling of the two "isolated" $S = \frac{1}{2}$ moieties. Parallel and perpendicular mode X-band spectra of frozen solutions were simulated using the full interaction spin Hamiltonian [considering only the ground state of the Mn dimer (Mn2) and the free radical (rad) spins]:

$$\hat{H}_{pair} = \hat{S}_{rad} \cdot (\mathbf{J_d} - J'\mathbf{1}) \cdot \hat{S}^0_{Mn2} + \sum \mu_B \hat{S}_j \cdot \mathbf{g}_j \cdot \mathbf{B} + \sum \hat{S}^0_{Mn2} \cdot \mathbf{A}_i \cdot \hat{I}_i$$

with j = rad, Mn2; i = Mn(III), Mn(IV). $\mathbf{J_d}$ is the anisotropic (dipolar) coupling matrix, J' is the isotropic exchange, **1** is the unitary matrix, and the Mn hyperfine interaction is included as this is a potential mechanism for singlet-triplet mixing. The effect of J' on EPR spectra is investigated by systematic simulation of parallel and perpendicular mode spectra and monitoring the behaviour of singlet-triplet transitions. The authors note that parallel mode is more sensitive to changes in J' because the otherwise intense $\Delta M_S = \pm 1$ transitions are attenuated. Although such transitions are not observed in **21–23**, this can still provide upper or lower limits for J'. $\mathbf{J_d}$ – magnitude and orientation – can in principle be determined from the half-field transitions. For complexes **21** and **23**, J' is found to be significantly larger than the microwave quantum and hence these can be analysed in the strong exchange limit, consistent with the $J' = -1.1$ and -2.8 cm^{-1} values, respectively, found from magnetic susceptibility studies. There is a significant difference in the relative intensities of the half-field ($g = 4$) and $g = 2$ regions of the spectra between these two complexes, implying a significantly smaller anisotropic coupling for **21** despite the shorter Mn2. . .rad distance, *cf.* **23**. This is found to be because $\mathbf{J_d}$ is unexpectedly large for **23** given its inter-spin separation (see below). No significant half-field signal is found for **22** and no singlet-triplet transitions are observed, and a much smaller $|J'|$ of *ca.* 0.02 cm^{-1} is concluded from simulation; this species also exhibits the smallest anisotropic coupling of the series. The dipolar couplings are calculated based on the known inter-spin distances (from X-ray crystallography) using a three-spin point model:

$$\hat{H}_{dipole} = (\mu_0 \mu_B^2 / 4\pi) \sum_{i=1,2} (g^0_{Mn2} g_{rad} / r^3) K_i \times \left(S^0_{Mn2} \cdot S_{rad} - 3 \left(S^0_{Mn2} \cdot r_{i,rad} \right) \left(S_{rad} \cdot r_{i,rad} \right) \right)$$

where $g^0_{\mathrm{Mn2}} = \sum_i \mathrm{K_i} g_i$ is the g value of the manganese dimer, and $\mathrm{K_i}$ are the projection coefficients for Mn(III) and Mn(IV). The calculated dipolar interactions for **21** and **23** (and their relative magnitudes) are consistent with the X-ray structures, and also give some information on the orientations of the nitroxyls, while the calculated value for **22** is much too small. The authors

conclude that the assumption that the radical spin is localized on the N–O moieties may not be valid and that spin density leaks onto the aryl spacer.

5 Mixed *d*/*f*-Block Radicals

There is one report of an EPR study of a mixed *d*/*f*-block system, for the pair of complexes $(NMe_4)[LnNi_6(pro)_{12}](ClO_4)_4$ (Hpro = proline) where Ln = Gd or La.[58] These structures consist of an octahedron of Ni(II) ions arranged about the trivalent lanthanide ion. Using a Kambé approach to analyse magnetic susceptibility data for the complex containing the f^7 Gd(III) ion, assuming only Gd...Ni and nearest-neighbour Ni...Ni interactions, the authors conclude that there is a five-fold orbitally degenerate $S = 13/2$ ground state – a strictly frustrated system. When Ln is the diamagnetic f^0 La(III) ion, weak antiferromagnetic exchange is observed between the Ni(II) ions. The Gd complex only gives an EPR transition at $g \approx 2$, and the upper limit of a ZFS is estimated. In contrast, the La complex is EPR silent at X-band but gives only two features at high frequency (*ca.* 150–500 GHz). The authors assign the low-field transition as the $\Delta M_S = \pm 2$ of a spin triplet and the high-field transition as a double-quantum transition, although they do not justify this assignment. From a frequency-resonance field plot they determine $|D| = 5.5$, $E = 0.8$ cm^{-1} for an $S = 1$ state. They conclude that the magnetic exchange is much less in magnitude than the single-ion anisotropy in this complex.

6 Biological Systems

6.1 Methods. – Pulsed electron-electron double resonance (ELDOR) or double electron-electron resonance (DEER) has become a widely employed technique used to examine distances between paramagnetic centres and in biological systems these centres are often nitroxide-based and introduced *via* chemical modification. Application of pulsed ELDOR to pairs of intrinsic metal-centred paramagnets has been undertaken by Bittl's group, and their prototypical examples were an as-isolated form of a [NiFe] hydrogenase and a $[3Fe\text{-}4S]^+$ cluster.[59] These oligomers introduced the additional factors (compared to nitroxides) of significant *g*-value anisotropy and a resultant spin, in the case of the latter, derived from magnetic exchange, wherein spin projection needs to be considered. The ELDOR spectra for the $[3Fe\text{-}4S]^+$ and [NiFe] centres in the hydrogenase from *D. vulgaris* Miyazaki F gave an experimentally observed dipole frequency of 8.5 MHz, which was larger than anticipated for the known inter-cluster distance from X-ray diffraction of 21.4 Å, assuming two point dipoles. Considering spin projection, the authors showed that the Fe ion of the $[3Fe\text{-}4S]^+$ cluster closest to the [NiFe] cluster had a large positive spin projection factor, which itself led to the calculation of a spin mixing parameter, α, that can also be determined independently from analysis by Mössbauer spectroscopy. Hence a further conclusion *via* values of α was that the [3Fe-4S] ferredoxin from *Azotobacter vinelandii* and that from the hydrogenase of the present study were very similar.

The Frankfurt group led by Prisner have introduced a method based on pulsed EPR and T_1 relaxation times to extract individual components from overlapping spectra. The method, termed relaxation filtered hyperfine (REFINE) spectroscopy[60] was applied to mitochondrial complex I, which is a multi-subunit, membrane-bound protein from the respiratory chain and contains several Fe-S centres. In particular the iron-sulfur cluster designated N2 has EPR signals that overlap significantly with other signals from this type of cluster. The method utilises an inversion-recovery filter, and a filter time T_F is defined such that this is the time at which the inversion recovery amplitude is zero, and no Hahn echo is observed in the pulsed detection sequence. Thus, for samples with components having different T_F values, individual spectra can be extracted from the mixture. It is suggested that a 2-dimensional time *versus* magnetic field sequence can be employed, without necessarily determining accurate T_F values for the individual components, to deconvolute spectra. A powerful extension of the method was demonstrated by applying it to ESEEM spectra with the results that it was shown that cluster N1 contains a ferredoxin [2Fe-2S] type cluster interacting with a peptide backbone nitrogen atom and that cluster N2 shows no direct bonding to nitrogen atoms.

6.2 Nitrogenases. – Hoffman and Seefeldt have embarked on a series of studies of intermediates in nitrogenase reactivity and have reviewed substrate interactions with the active site of nitrogenase.[61] They used ENDOR and ESEEM at Q-band on the $S = \frac{3}{2}$ states of protein-bound compared with extracted FeMo-cofactor to assess whether the unassigned electron density located by X-ray crystallography in the centre of the [$MoFe_7S_9$:homocitrate] cluster of nitrogenase might belong to a nitrogen atom.[62] They deduce from a detailed comparative study that observed $^{14/15}N$ responses all arise from protein-bound nitrogen nuclei and not from the cofactor. Hence they assert that unless the proposed nitrogen atom in the centre of the cluster is magnetically uncoupled (*i.e.* hyperfine splitting $\sim$0 MHz, where the authors claim an experimental detection limit for $A(^{14}N)$ on the $S = \frac{3}{2}$ system of $\sim$0.1 MHz) from the electron spin system, then in their standard preparative conditions there is no nitrogen atom at the centre of the cofactor.

Rapid freeze experiments on reduction of propargyl alcohol ($HC{\equiv}C–CH_2OH$) by nitrogenase trapped an intermediate $S = \frac{1}{2}$ state, which was investigated by c.w. and pulsed ^{13}C ENDOR, and using Mims and stochastic-field modulated methods for $^{1,2}H$ ENDOR at Q-band frequency.[63] Using the derived hyperfine interaction matrices an organometallic, doubly reduced, side-on bonded allyl alcohol product is proposed.[64] Wild-type and mutants of nitrogenase, designed for early (*e*), middle (*m*) and late (*l*) stage studies of turnover using nitrogen (N_2), methyldiazene, ($CH_3N{=}NH$) and hydrazine (N_2H_4), respectively were investigated by ^{15}N Mims-pulsed and ^{1}H c.w. ENDOR at Q-band frequency to provide evidence for the structure of trapped intermediates. These were assigned from single- and double-labelling with ^{15}N, and were consistent with a cluster-substrate intermediate. Work on hydrazine trapping was extended[65] and turnover of a double mutant nitrogenase, which

also involved EPR signals from a $S = \frac{3}{2}$ spin system, produced a freeze-trapped $S = \frac{1}{2}$ state with a rhombic EPR signal (g-values: 2.09, 2.01, 1.93) optimised at pH = 7.4, showing the same Curie-Law behaviour to that of the resting state EPR signal. ^{15}N Mims pulsed ENDOR at Q-band with samples of isotopically enriched hydrazine showed that a hydrazine-derived species was incorporated at the FeMo-cofactor and the low field g-value carried a ^{15}N hyperfine interaction of 1.5 MHz. These workers also studied dihydrogen evolution using ^{1,2}H ENDOR on another variant protein that allowed a $S = \frac{1}{2}$ state to be trapped during reduction of protons to H_2.[66] Hyperfine matrices were determined from 2-dimensional field-frequency plots that gave a large isotropic hyperfine coupling $A_{iso} \sim 23$ MHz, and hence deduced to be bound to the cofactor, but in addition the two hydrogen atoms have the same principal values of their hyperfine matrices, and so are possibly two chemically equivalent bound hydride ions.

Newton, Fisher and co-workers have purified nitrogenase proteins from *Gluconacetobacter diazotrophicus*, a sugar-cane colonizing bacterium and obtained characteristic c.w. EPR spectra at X-band frequency reporting results from MoFe and Fe proteins.[67] The EPR signals from component 2 of *G. diazotrophicus* (Gd2) were at g-values = 4.16 (4.27), 3.69 (3.64) and 2.01 (2.01), where the values in parentheses are those from dithionite-reduced protein from *A. vinelandii*, and additional features at $g = 5.09$ and 3.96, which were also present in whole cells, crude extracts and throughout the purification procedure. The $S = \frac{1}{2}$ signal of the Fe protein was reported to be identical to that from the protein isolated from *A. vinelandii*. In a separate study[68] using nitrogenase from *A. vinelandii*, this group investigated turnover under carbon monoxide, which has the effect of removing the characteristic $S = \frac{3}{2}$ signal and producing several new ones. These signals have been investigated for a series of mutant MoFe proteins, but no new parameters were observed, which implied that no new CO binding sites had been generated in the variants. Ribbe *et al.* identified two [8Fe-7S] P-cluster variants of nitrogenase, which they characterised by analysis, activity and a range of spectroscopic techniques including c.w. EPR at X-band and showed $S = \frac{1}{2}$ signals.[69] Petersen and co-workers investigated Mn^{2+}-adenosine nucleotide complexes in the presence of the iron protein of nitrogenase from *Klebsiella pneumoniae* by c.w. EPR and 2D-ESEEM at X-band frequency.[70] By changing the redox state of the Fe-protein and detecting conformational rearrangements directly at the nucleotide binding site it was suggested that the Fe-S cluster communicates with that site.

6.3 Copper. – Copper incorporation (reconstitution) in the multi-copper oxidase known as CueO (formerly yacK) followed by c.w. X-band spectroscopy did not show any resonances in addition to those attributed to the type 1 and type 2 centres.[71] The plasma-membrane, multi-copper oxidase protein Fet3p in *Saccharomyces cerevisiae* also contains one each of type 1, type 2 and bimetallic type 3 sites and is essential for iron uptake in yeast. A study of mutants, by Solomon *et al.* using EPR, CD and MCD spectroscopies, reported no unusual EPR signatures of the resultant tricopper (type 2 plus type 3) cluster.[72] In *Rhus*

vernicifera laccase a similar set of copper centres is found made up of the three types of copper sites. Multi-frequency c.w. EPR at X- and Q- bands and at 285 GHz were used to study the trimetallic active site and DFT calculations of models were used to estimate isotropic magnetic exchange constants (J), but the EPR data were not able to provide experimental support for the theoretical results.[73] The exchange coupling between the high spin Fe(III) haem o_3 and Cu_B(II) in quinol oxidase (cytochrome bo_3) from *Escherichia coli* was studied by c.w. X-band EPR and variable temperature variable field (VTVF) MCD by Thomson *et al.*[74] Both parallel and perpendicular mode detection were used in the EPR spectra and spectrum simulations were used to show that the EPR responses could only arise from a weakly coupled (by anisotropic exchange) interaction with $|J| \sim 1\ \mathrm{cm}^{-1}$, which led to a "four-level" energy state model. Four anion-treated forms of cytochrome bo_3 were studied: fluoride, azide, chloride and formate as well as the oxidised form and a spin-Hamiltonian of the form:

$$\hat{H} = [\tilde{g} \cdot \beta \cdot \boldsymbol{H} \cdot \hat{S} + D(\hat{S}_z^2 - \hat{S}^2/3) + E(\hat{S}_x^2 - \hat{S}_y^2)]^{Fe} + [\tilde{g} \cdot \beta \cdot \boldsymbol{H} \cdot \hat{S}]^{Cu} + \hat{S}^{Fe} \cdot \tilde{J} \cdot \hat{S}^{Cu}$$

was employed. The EPR spectra in each case were very similar to each other, and it was suggested that overlap of magnetic orbitals between iron and copper was hindered and hence was the cause of the structural similarity in these forms. The authors went on to consider published magnetic and spectroscopic data for the coupled Fe-Cu pair in cytochrome *c* oxidase and concluded that the interpretation of the data requiring a strongly coupled pair with a resultant $S' = 2$ ground state is not necessarily correct. In addition, it was suggested that the "four-level" model might have wider applicability for instance in the iron-nitrosyl ($S = \frac{3}{2}$) and semiquinone $Q_A^{-\bullet}$ radical in Photosystem II. Strong magnetic exchange leading to EPR-silent states as measured at X-band frequency has been reported for the coupled cytochrome b_3 with Cu_B coupling in a NO reductase homologue from *Roseobacter denitrificans*.[75]

6.4 Manganese (Excluding Photosystems). – Multifrequency (X-, Q- and W-band) measurements on the antiferromagnetically coupled mixed valence Mn^{III}-Mn^{IV} and Mn^{II}-Mn^{III} states of di-manganese catalase from *Thermus thermophilus* together with some related low molecular weight analogues have been reported as part of a special issue of *Magnetic Resonance in Chemistry* on High-field EPR in Biology, Chemistry and Physics.[76] Data analysis used a simplified spin-Hamiltonian to exchange couple the dimetallic:

$$\hat{H} = -2J\hat{S}_1 \cdot \hat{S}_2 + \tilde{g}_1 \cdot \beta \cdot \boldsymbol{H} \cdot \hat{S}_1 + \tilde{g}_2 \cdot \beta \cdot \boldsymbol{H} \cdot \hat{S}_2 + \hat{S}_1 \cdot \tilde{a}_1 \cdot \hat{I} + \hat{S}_2 \cdot \tilde{a}_2 \cdot \hat{I}_2 + \hat{S}_1 \cdot \tilde{d}_1 \cdot \hat{S}_1 + \hat{S}_2 \cdot \tilde{d}_2 \cdot \hat{S}_2$$

where the terms have their usual meaning, with lower case letters defining single centre interactions. Also, a spin-coupled Hamiltonian was employed:

$$\hat{H} = \tilde{G}_1 \cdot \beta \cdot \boldsymbol{H} \cdot \hat{S} + \hat{S}_1 \cdot \tilde{A}_1 \cdot \hat{I} + \hat{S}_2 \cdot \tilde{A}_2 \cdot \hat{I}_2$$

where upper case letters represent resultant interactions derived from single centre interactions by spin projection factors defined for a two-centre spin system as:

$$c_1 = \frac{S_1(S_1+1) - S_2(S_2+1) + S(S+1)}{2S(S+1)} \text{ and}$$
$$c_2 = \frac{S_2(S_2+1) - S_1(S_1+1) + S(S+1)}{2S(S+1)}$$

and where:

$$G = c_1 g_1 + c_2 g_2 + \tfrac{c_1 c_2}{5J}(g_1 - g_2)[(3c_1+1)d_1 - (3c_2+1)d_2]$$
$$A_1 = c_1 a_1 - \tfrac{a_1}{5J} c_1 c_2[(3c_1+1)d_1 - (3c_2+1)d_2]$$
$$A_2 = c_2 a_2 - \tfrac{a_2}{5J} c_1 c_2[(3c_1+1)d_1 - (3c_2+1)d_2]$$

Iterative fitting of simulated spectra across all three frequencies was used to obtain a final set of spin-Hamiltonian parameters. The spectra for $Mn^{III}Mn^{IV}$ ($c_1 = 2$ for $S_1 = 2$, and $c_2 = -1$ for $S_2 = \frac{3}{2}$) all showed overall 16 line patterns and hence $|J| \gg |d|$, whereas for $Mn^{II}Mn^{III}$ ($c_1 = 7/3$ for $S_1 = 5/2$, and $c_2 = -4/3$ for $S_2 = 2$) complex, broad spectra were reported. New data (tabulated below) and those from the literature were analysed and compared with the results of DFT calculations.

Enzyme	Anisotropy	g	$-A$ (Mn^{III})/ mT	A (Mn^{IV})/ mT	g_{iso}	$-A_{iso}$ (Mn^{III})/ mT	A_{iso} (Mn^{IV})/ mT
Mn^{III}-	X	2.0048	15.2	8.0			
Mn^{IV}	Y	2.0040	14.7	8.3	1.9988	13.5	8.5
catalase	Z	1.9876	10.7	9.1			
			$-A$ (Mn^{II})/ mT	A (Mn^{III})/ mT		$-A_{iso}$ (Mn^{II})/ mT	A_{iso} (Mn^{III})/ mT
Mn^{II}-	X	1.935	19.3	8.0			
Mn^{III}	Y	1.995	18.4	7.8	1.982	21.2	7.8
catalase	Z	2.016	25.6	7.7			

The exchange coupling switched from the strong-exchange limit in Mn^{III}-Mn^{IV} to one in which zero-field splitting could not be ignored because there was only small exchange coupling for Mn^{II}-Mn^{III}.

Solvent-bridging in di-manganese(II) phophoesterase has been investigated by c.w. X-band EPR spectroscopy allied to spectrum simulation by assigning spectra to the resultant $S' = 2$ state of an exchange coupled pair using Boltzmann weighting of transitions from a full matrix diagonalisation treatment of the spin-Hamiltonian:

$$H = -2J\hat{S}_1 \cdot \hat{S}_2 + \hat{S}_1 \cdot \tilde{d}_{12} \cdot \hat{S}_2 + \sum_{i=1}^{2}[\hat{S}_i \cdot \tilde{D} \cdot \hat{S}_i + \tilde{g} \cdot \beta \cdot \boldsymbol{H} \cdot \hat{S}_i + \beta_n \cdot \tilde{g}_n \cdot \boldsymbol{H} \cdot \hat{I}_i + \hat{S}_i \cdot \tilde{A}_i \cdot \hat{I}_i]$$

An exchange coupling constant of $J = -2.7 \pm 0.2$ cm^{-1} was determined, consistent with a hydroxide and carboxylate bridge, and a rhombic zero-field splitting ($D = -0.055$ and $E = -0.0067$ cm^{-1}) are reported.

The sulfate-oxidising enzyme system in *Paracoccus pantotrophus* is comprised of four periplasmic proteins (SoxXA, SoxYZ, SoxB and SoxCD), mediating cytochrome *c* reduction dependent on hydrogen sulfide, sulfur, thiosulfate and sulfite, although separately each protein is inactive. A variable temperature X- and Q-band EPR study[78] of the di-manganese SoxB protein by Lubitz *et al.* also used a spin-Hamiltonian of the form above relying on simulations with XSophe and Easyspin software as well as some in-house routines, and overall parameters were obtained from single ion values (for g, D and A interactions) by spin projection. The rich hyperfine structure (11 lines) was filtered out from broad background resonances. The analysis was simplified by assuming that the g-value and zero-field splitting contributions of the two manganese ions were identical, that the g-value was isotropic (refined to 1.9 ± 0.01), that the dipole tensor ($\tilde{d}_{12}$) was axial with its largest component co-parallel with the Mn–Mn direction, and that the hyperfine coupling matrix was isotropic (8.12 ± 0.1 mT). Features were identified for each of the resultant $S' = 1$, $S' = 2$ and $S' = 3$ spin states and gave $J = -7 \pm 1$ cm^{-1}. The single ion zero-field splitting tensor was set to have its largest principal component at an angle θ to the Mn–Mn direction and the inter-metal distance was also refined *via* the dipolar tensor, where:

$$\tilde{d}_{12} = \frac{\beta^2}{r^3}\left(\tilde{g}_1\tilde{g}_2 - \frac{3(g_1\underline{r})(\underline{r}g_2)}{r^2}\right)$$

whereupon the remaining parameters were determined as $r_{\mathrm{Mn-Mn}} = 3.4 \pm 0.1$ Å, $D = -0.09$ cm^{-1}, $E/D = 0$ and $\theta = 15^\circ$.

6.5 Diiron (Including 2Fe-2S). – The aldehyde oxidoreductase from *Desulfovibrio gigas* contains two $[2\mathrm{Fe\text{-}2S}]^{2+/1+}$ clusters and a molybdenum cofactor, and when all three sites are at paramagnetic oxidation levels there are splittings in the X- and Q-band EPR spectra resulting from inter-centre spin-spin couplings.[79] This study was facilitated by the observably different EPR linewidths of the three centres and their structural arrangement within the enzyme. The theory for this analysis followed from a previously published method by the same group in which local spins were considered to interact by a dipolar mechanism in which the magnetic moment on each individual metal site was used. Variable temperature measurements were needed to obtain regimes of T_1 in which the additional dipolar splittings could be observed. Thus spin-spin interactions between the Mo centre and the proximal $[2\mathrm{Fe\text{-}2S}]^{1+}$ cluster was only seen in the splitting of Mo(V) EPR signals. In combination with the reported X-ray crystal structure these EPR results were used to propose an electron-transfer pathway within the enzyme.

The study by EPR spectroscopy of iron-sulfur clusters in the NADH:Ubiquinone oxidoreductase (complex I) of *E. coli* has continued (see also Section 6.6).

Uhlmann and Friedrich[80] used site-directed mutants to show that the previously reported and spectroscopically unusual "N1c" with g-values = 1.92, 1.94 and 2.00 does not derive from a new [2Fe-2S] cluster, but from cluster N1a. Verkhovskaya *et al.*[81] propose that "N1c" is a degradation product of other [2Fe-2S] clusters in complex I. Daldal *et al.* used angular variation of X-band spectra of layered membrane samples of cytochrome bc_1 from *Rhodobacter capsulatus* to investigate the [2Fe-2S] cluster, in particular to ascertain the orientation of the cluster in mutations that led to changes in mid-point potential for the redox active cluster.[82] A model of the quinone oxidation site was produced from these EPR data.

The $S = \frac{1}{2}$ signal from the mixed valence di-iron cluster in recombinant ferritin from *Pyrococcus furiosus* expressed in *E. coli* was used in a redox titration to determine mid-point potential.[83] The state had all of its g-values below 2.0, did not saturate up to 200 mW and down to 9 K and broadened out to become undetectable above 20–25 K. However, a broad signal with unusual temperature dependence in the range 6.8 to 44 K also appeared at intermediate potentials, but was not seen using parallel mode detection. The signal was tentatively ascribed to a modified mixed valence di-iron centre resulting from ferritin biosynthesis in the heterologous host. The narrower signals were stated to define the stable prosthetic group of this protein and to be part of a three redox state cycle.

Recombinant *E. coli* biotin synthase (BioB), which converts dethiobiotin into biotin by inserting a sulfur atom in a S-adenosylmethionine (SAM)-dependent reaction and contains a [2Fe-2S] cluster, is inactive *in vitro* without the addition of exogenous iron. Anaerobic reconstitution of BioB with Fe^{2+} and S^{2-} produces a form that contains both a [2Fe-2S] and a [4Fe-4S] cluster and a combination of EPR (X-band) and Mössbauer spectroscopies have been used to monitor turnover.[84] The EPR data confirmed that $S = \frac{1}{2}$ states of the Fe-S clusters are generated during turnover, and that radical production takes place. In addition cluster degradation of the [2Fe-2S] cluster was seen to accompany turnover.

6.6 Other Iron–Sulfur Centres. – The "radical-SAM" super-family of enzymes is thought to have more than 600 members and these contain iron-sulfur clusters and S-adeosylmethionine (SAM or AdoMet). Pyruvate formate-lyase (PFL), an enzyme involved in anaerobic glucose metabolism and involving a long lived ($t_{\frac{1}{2}} \geq 24$ h under anaerobic conditions) glycyl radical, was chosen by Broderick *et al.*[85] as the basis to make a generic study of this family by EPR and ENDOR spectroscopy, and using an activating system that included an activating enzyme (AE), SAM, Fe(II) and reduced flavodoxin. No crystal structure had yet been reported for PFL-AE. c.w. X-band measurements were used to assess activity and to follow turnover under a variety of conditions, and Q-band pulsed ENDOR spectra were obtained as field-frequency plots using isotopically enriched versions of SAM with ^{13}C, ^{17}O and ^{15}N. A proposed structural model and mechanism were built using a point dipole approximation to analyse the results in conjunction with published Mössbauer data, and in comparison with reported crystal structures

on three other members of the radical-SAM super-family. Thus a site-differentiated [4Fe-4S] cluster is proposed to be chelated at one iron by a carboxyl oxygen and amino nitrogen of SAM to give a five-membered ring, and the sulfur atom of the ligand interacts with a bridging sulfide bonded to the iron in the cluster. Also within this super-family, c.w. X-band EPR spectra at 13 K showed that lipoyl synthase from *E. coli* binds two [4Fe-4S] clusters, distinguished by their g-values, but Mössbauer data were not able to achieve this distinction.[86]

The proton-pumping NADH-quinone oxidoreductase from *E. coli* contains nine iron-sulfur clusters of which eight are found in its mitochondrial counterpart, complex I. These clusters can be individually deactivated by mutation of the binding motif using replacement of four cysteine residues with alanine. Cicchillo *et al.*[87] used reducing conditions to produce EPR signals in the "$g = 2$" region, and determined that a set of rhombic signals at *g*-values 1.91, 1.94 and 2.05, visible between 6 and 20 K, were assigned to cluster N1c and hence confirmed that it is a [4Fe-4S] cluster that ligates to the N1c motif, rather than a [2Fe-2S] cluster as had been reported elsewhere. Work on complex I by Verkhovskaya *et al.*[88] followed activation by detergent and phospholipids by c.w. X-band EPR spectroscopy and suggested conformational rearrangements were involved and associated with two [4Fe-4S] clusters.

The characteristic $S = \frac{1}{2}$ EPR signal for [3Fe-4S] clusters was used to identify an unexpected variation within three minor Fe-S proteins, designated V-I, V-II and V-III, found whilst purifying recombinant *Bacillus thermoproteolyticus* ferredoxin (BtFd) from *E. coli*.[89] A crystal structure at 1.6 Å resolution of the BtFd-CoA complex (V-II) showed that each complex in the asymmetric unit comprised a [3Fe-4S] cluster coordinated by 3 cysteines, and that the polypeptide chain was superimposable on the original [4Fe-4S] cluster of BtFd. However, the fourth cysteine of this binding domain was rotated away towards the surface of the protein and formed a disulfide bond with the terminal sulfhydryl group of CoA.

Hagen *et al.*[90] have performed a detailed multi-frequency (X-, Q- and D-bands) EPR study on the $[4Fe\text{-}4S]^{3+}$ oxidation level ($S = \frac{1}{2}$) of a series of seven high potential iron-sulfur proteins (HiPIPs) from six microbial sources. The *g*-values were found to be frequency independent, but the form of the spectra was subject to significant *g*-strain broadening, and rapid-passage effects dominated the Q- and D-band spectra. Multi-component g-strain simulations at X-band identified three to four discernible species, which were assigned to valence isomers, *i.e.* the mixed valence pair $[Fe^{II}–Fe^{III}]$ can be in any one of six positions in the cluster. The results were compared to a model in the literature proposed from paramagnetic NMR studies.

Mutants of the [4Fe-4S]-containing Ech hydrogenase from *Methanosarcina barkeri* were probed by c.w. X-band EPR spectroscopy at 10 K in a study[91] of the $S = \frac{1}{2}$ signals of the reduced clusters. The spectra were used to identify the cluster giving a $g = 1.89$ signal as the proximal cluster located in EchC and the $g = 1.92$ signal arose from one of the clusters of subunit EchF. Barton *et al.*[92] used c.w. X-band EPR at 10 K in conjunction with the results of

electrochemistry on DNA-modified electrodes to study DNA repair glycosylases containing [4Fe-4S] clusters. A functional role for the iron-sulfur clusters was established and characteristic EPR signals identified that both $[4Fe\text{-}4S]^{3+}$ and $[3Fe\text{-}4S]^{1+}$ were present. A multi-spectroscopic approach showed that L-serine deaminase from *E. coli* uses a [4Fe-4S] cluster, and the dithionite-reduced reconstituted protein has typical parameters of: $g_{\|} = 2.03$ and $g_{\perp} = 1.93$, but treatment of the reduced protein with L-serine resulted in broadening of the former signal, indicative of a direct interactions of the amino acid with the cluster.[93]

Weiner *et al.* used EPR-monitored (X-band, liquid helium temperatures, $S = \frac{1}{2}$ signals) redox titrations in an investigation of the environment surrounding iron-sulfur cluster 4 of *E. coli* dimethyl sulfoxide reductase.[94] The group showed that this cluster is the first electron acceptor in the relay defined by four such clusters and that the [3Fe-4S] form of this cluster can act as a barrier to electron transfer by virtue of its high redox potential. Weiner and co-workers have also used EPR spectroscopy, redox potentiometry and protein crystallography to characterise the novel [4Fe-4S] cluster (designated FS0) of nitrate reductase A from *E. coli*,[95] which contains one histidine and three cysteine ligands. At temperatures of less than 15 K at X-band frequency EPR signals at effective *g*-values 5.023 and 5.556 were detected, which varied as a function of redox potential, and the midpoint (standard) potential of both signals was −55 mV at pH = 8.0. The signals were assigned to a $S = \frac{3}{2}$ ground state of a $[4Fe\text{-}4S]^{1+}$ cluster.

The characterisation of a new formate dehydrogenase (FDH) from the sulfate-reducing organism *Desulfovibrio alaskensis* NCIMB 13491 by EPR spectroscopy following dithionite reduction showed two ferredoxins with sets of *g*-values of: 1.882, 1.946 and 2.046 (cluster I) and 1.868, 1.931 and 2.066 (cluster II), with evidence for additional iron-sulfur clusters.[96]

^{57}Fe-pulsed Davies-ENDOR at X- and W-bands have been used to probe the [4Fe-4S] cluster in the heterodisulfide reductase (Hdr) from *Methanothermobacter marburgensis*, which catalyzes the reversible two electron reduction of the mixed disulfide between coenzyme M and coenzyme B.[97] Measurements on Hdr-CoM indicated that the cluster was oxidised, *i.e.* $[4Fe\text{-}4S]^{3+}$, and that there was direct interaction of the cluster with the substrate. The results were contrasted with those reported elsewhere for a ferredoxin:thioredoxin reductase (FTR) that also catalyses a disulfide cleavage, where the latter enzyme has significant anisotropy of ^{57}Fe hyperfine coupling at the unique iron site, but also $g_{av} > 2.0$ is reported for FTR (typical of $[4Fe\text{-}4S]^{3+}$ clusters) whereas $g_{av} < 2.0$ for Hdr-CoM. In addition, it was noted that the cluster-binding cysteines were not conserved between the two proteins and possible analogies to the multiple binding sites found in radical-SAM enzymes were also suggested. Walters and Johnson have reviewed the structural and spectroscopic studies on ferredoxin:thioredoxin reductase,[98] collecting together data from electronic absorption, EPR, ENDOR, VT-MCD, resonance Raman and Mössbauer spectroscopies. Mechanisms for the catalytic cycles of FTR and

Hdr were suggested and open questions were posed and future prospects for research were identified.

Dual mode c.w. X-band spectra at liquid helium temperatures were used as part of the characterisation of MOCS1A, an oxygen-sensitive iron-sulfur protein involved in human molybdenum cofactor biosynthesis.[99] In addition to signals in the "$g = 2$" region, signals at effective g-values 9.4 in both modes of detection were assigned as being characteristic of a $S = 2$ $[3Fe\text{-}4S]^0$ cluster.

A [4Fe-4S] cluster with g-values 2.067, 1.933 and 1.89 measured at X-band at 20 K was identified from isolation of the photosynthetic reaction centre *Heliobacterium modesticaldum* (HbRC) and also in whole cells and isolated membranes.[100] Illumination produced a complex spectrum consistent with exchange interaction between two iron-sulfur clusters.

6.7 Photosystems. – Britt *et al*. have reviewed[101] recent pulsed EPR studies of the Photosystem II oxygen-evolving complex (PSII OEC) from a mechanistic viewpoint and begin their review acknowledging the debt owed to Jerry Babcock by workers in the field of EPR of PSII, noting his guidance, enthusiasm and significant contributions to the area. Substrate and cofactor interactions were highlighted in the context of proposed mechanisms of action, with a suggestion that substrate water molecules bind early in the S-state cycle, for which pulsed EPR data are limited to the lower S-states, S_0–S_2. Blondin *et al*. report on c.w. X-band spectra of IR sensitive, untreated PSII and MeOH- and NH_3-treated PSII from spinach in the S_2 state.[102] Spectrum simulation used co-parallel g- and Mn-hyperfine matrices to obtain principal values that indicated a $1 \times Mn^{III}$-$3 \times Mn^{IV}$ cluster and these were in good agreement with previously published values. A magnetic exchange coupling scheme involving four J-values was explored against derived spin densities to yield antiferromagnetic interactions with values between -290 and -130 cm^{-1}, giving a $S = \frac{1}{2}$ ground state and first excited state of $S = \frac{5}{2}$ at $+30$ cm^{-1} responsible for a $g_{eff} = 4.1$ signal.

c.w. EPR, electron-spin-echo (ESE)-detected field swept and electron spin echo envelope modulation (ESEEM) spectra at X-band frequency were reported on the effect of adding isotopically labelled azide (^{15}N-^{14}N-N^-) to PSII membrane samples (BBY preparation) with or without chloride.[103] Analysis of the results showed that a binding site close to the manganese cluster was competitive for azide and chloride, implying that chloride is bound proximally to the cluster, and it was also shown that inhibition induced by azide could be partially recovered by addition of bicarbonate. Britt and co-workers have also demonstrated, by c.w. EPR and ESEEM spectroscopies, that the presence or absence of the 33 KDa manganese-stabilising protein, which limits access of small molecules to the metal site, bound to the lumenal side of PSII close to the Mn_4Ca cluster, has no effect in the number or distance of deuterons magnetically coupled to manganese after equilibration with D_2O.[104] The samples of PSII were trapped in the dark stable S_1 state prior to illumination at 200 K for

ESEEM measurements. Analysis of modulation depths led to estimation of distance between deuteron and manganese of 2.5–2.6 Å. Glycerol-treated samples were also investigated, which led to changes in the "$g = 4.1$" signal, but it was shown that unlike treatment with smaller alcohols such as MeOH, there was no direct binding of glycerol to the manganese site. It was suggested that the 33 KDa protein might control access to higher S-state transitions in order to manage possible side reactions. This group has also investigated the calcium-binding site of the OEC of PSII using ^{87}Sr ESEEM spectroscopy in conjunction with spectrum simulation and DFT calculations.[105] A stimulated echo modulation function for the $I = 9/2$ nucleus in the absence of nuclear quadrupole effects was derived following the method of Dikanov and co-workers. However, the analysis was extended using a numerical diagonalisation procedure to include a non-zero quadrupolar interaction, the results of which were compared directly with quadrupole couplings calculated by DFT methods, for both ^{43}Ca and ^{87}Sr. It was concluded that the DFT method overestimated these couplings by up to a factor of two. Use of a simple point dipole approximation on the modulation depth gave a Mn-Sr(Ca) distance of 4.5 Å, which was converted to a range of 3.8 to 5.0 Å, if a tetrametallic magnetic model for the cluster was considered. However, this range defines an upper bound because the effect of nuclear quadrupole coupling was not included in those calculations.

Q-band pulsed ESE-detected field swept and inversion-recovery spectra on PSII membranes have been used to measure the electron spin-lattice relaxation times, T_1, for the S_0 state of the OEC, in comparison with two di-manganese complexes.[106] The relaxation times in the S_0 state were measured between 4.3 to 6.5 K and indicated that an Orbach mechanism exists with a first excited state at 21.7 ± 0.4 cm^{-1} above the ground state. ^{55}Mn pulsed ENDOR spectra at Q-band frequency have been reported for both S_2 and S_0 states,[107] and these are taken to indicate that all four manganese ions are magnetically coupled. Principal, absolute values for the hyperfine interaction matrices in the two states are given below:

	S_2 state		S_0 state	
	$A_\perp$/MHz	$A_\parallel$/MHz	$A_\perp$/MHz	$A_\parallel$/MHz
Mn_A	235	265	270	200
Mn_B	185	245	190	280
Mn_C	310	265	320	400
Mn_D	175	230	170	240

The similarity in magnitude between the two sets of values led to the suggested assignment of Mn_4(III, III, III, IV) and Mn_4(III, IV, IV, IV) for the S_0 and S_2 states, respectively.

A series of inversion-recovery and microwave power saturation measurements on the tyrosine Y_D radical of PSII between 4 and 25 K have been

reported by a different group.[108] The dark stable S_1 and first turnover S_2 states were studied in sucrose and in ethyleneglycol-glycerol as cryo-protectants. A through-space dipolar relaxation model was shown to dominate and was only slightly temperature-dependent and was independent of S-state. A background exponential decay was an order of magnitude weaker and was temperature and S-state dependent, consistent with an interaction of $Y_D^{\bullet}$ and the manganese cluster over a range of *ca.* 30 Å.

X- and W-band c.w. EPR spectra at *ca.* 10 K have been used to probe the tyrosine Z radical and manganese cluster in the S_1 state.[109] Characteristic resonances with *g*-values of 2.019, ~2.00 and 1.987 were defined at W-band and were simulated by assuming that the manganese cluster had two low lying states, $S = 1$ and $S = 0$, with the former interacting with the $S = \frac{1}{2}$ state of the radical. Simultaneous fitting at both frequencies gave the following parameters (estimated errors on the last digit in parentheses) for the manganese cluster and for the ferromagnetic exchange with the radical: $g_x = 2.0055(3)$, $g_y = 2.0043(2)$, $g_z = 1.992(3)$, $D = -0.048(2)\ cm^{-1}$, $\lambda = 0$, $J_x = -0.087(2)\ cm^{-1}$, $J_y = J_z = 0\ cm^{-1}$. The extracted parameters were of similar magnitude and so the authors stated that further data are required in order to define the various interactions with more certainty.

A series of pulsed X-band experiments, including ^{55}Mn-ELDOR on the S_2-state of the OEC of PSII have been reported,[110] and the broad peak found in the double frequency experiment is consistent, by spectrum simulation, with manganese hyperfine interactions determined from ^{55}Mn-ENDOR, and these are tabulated below, and show good agreement with the results given in reference 107.

	$A_\perp$/MHz	$A_\parallel$/MHz	$P_\parallel$/MHz
Mn_A	−232	−270	−3
Mn_B	200	250	−3
Mn_C	−311	−270	8
Mn_D	180	240	1

The hyperfine and nuclear quadrupole interactions were strongly correlated such that moving within a range of 10 MHz about the tabulated A-values could be compensated by changes in the *P* parameters and maintain the same degree of correspondence between simulated and experimental spectra. A random acquisition technique was used to measure the ENDOR response, wherein the radio-frequency field was not swept linearly, but was varied randomly within the required range in order to decrease local heating.

The heterogeneous nature of the multi-line EPR spectrum of the S_2-state of the OEC of PSII was shown to be manifest in two forms of EPR signal, and significantly it was demonstrated that MeOH favoured the narrow form on first turnover of the enzyme, as determined by c.w. X- band and Q-band EPR spectroscopy.[111] The effect was removed on subsequent turnovers and led to a

predominant broad form of the multi-line spectrum. ESEEM characterisation of the narrow form of the spectrum was also reported, and a structural model was proposed for the MeOH binding to the OEC.

X-band ESEEM spectroscopy of the S_2-state in the presence of $H_2{}^{17}O$ (final enrichment of sample 20-30%) showed modulations around the ^{17}O Larmor frequency at *ca.* 2 MHz and further features up to *ca.* 18 MHz assigned to ^{17}O, but only observed when the applied magnetic field was at the centre of the multi-line spectrum between effective g-values of 1.98 and 1.87.[112] Analysis of the data gave $A_{iso} \sim 5$ MHz and a quadrupole interaction >6 MHz, and it was suggested that this meant that water, rather than OH^-, was the bound species. c.w. and ELDOR studies have been reported on a mutant in which a glutamate proposed to act as a direct ligand to the manganese cluster was replaced by a glutamine.[113] The S_2-state spectra and the S_2-state to $Y_D^{\bullet}$ distance determined by ELDOR were unaffected by the modification, although redox potential and FTIR spectral data were changed relative to those of the unmodified OEC.

6.8 Nickel. – HYSCORE and ENDOR spectra at X-band frequency at liquid helium temperatures on two states, Ni-A (''unready'') and Ni-B (''ready'') of the [Ni-Fe] hydrogenase from *Desulfovibrio vulgaris* Miyazaki F, isolated and purified under aerobic conditions, showed that both have an exchangeable proton, but with different hyperfine coupling.[114] DFT calculations were used in the analysis and the proton was assigned to a bridging hydroxide ligand between Ni and Fe in Ni-B and either a differently bonded hydroxide or a hydroperoxide in Ni-A. A similar and very detailed experimental study of the reduced Ni-C (''active'') state has been reported by the same group,[115] and the problem of ambiguity of signs (in the choice of direction cosines) for the location of the non-exchangeable protons was discussed. Two strongly coupled protons were assigned to β-CH_2 of a ligating cysteine residue and a third, slightly more weakly coupled proton, was assigned to a different cysteinyl β-CH_2. D_2O exchange experiments showed the presence of hydride in the bridge between the iron and nickel centres. ^{14}N interactions were also detected and these were assigned to a histidine residue hydrogen-bonded to the cysteine with the strongly coupled (to the unpaired electron) protons.

S-, X-, Q- and D-band c.w. EPR spectra were used to examine the CO-dehydrogenase/acetyl-CoA synthase enzyme from *Moorella thermoacetica*, for which the identity of essential metal ions was not clear.[116] Ni, Cu and Zn had previously been implicated as having active roles as part of a heterodimetallic site, with proximal and distal positions relative to bridging to a [4Fe-4S] cluster. Using enzyme preparations with a wide range of Ni and Cu stoichiometries per dimetallic unit, followed by removal of the metal from the proximal site using selective chelators and then monitoring by EPR and EXAFS spectroscopy led to a consensus view of the active site. It was reported that the ''NiFeC'' EPR signal derived from a $[4Fe\text{-}4S]^{2+}$ ($S = 0$) cluster bridged to Ni^{1+} ($S = \frac{1}{2}$) that was itself bridged to a planar Ni^{2+} ($S = 0$).

6.9 Miscellaneous. – Ethanolamine deaminase from *Salmonella typhimurium* is coenzyme B_{12}-dependent and catalyses elimination of ammonia from aminoethanol to yield ethanal *via* production of a low spin Co^{II}-cobalamin and a carbon-centred deoxyadenosyl radical pair.[117] c.w. EPR and ESEEM spectroscopy at X-band frequency on the radical pair have been used to give a partial structural model for the active site and for the hydrogen atom abstraction event in the catalysis.

References

1. D. Collison and E.J.L. McInnes, *Specialist Periodical Reports Electron Spin Resonance Series*, B.C. Gilbert, M.J. Davies and D.M. Murphy (eds), Royal Society of Chemistry, Cambridge, 2002, **18**, 161.
2. D. Collison and E.J.L. McInnes, *Specialist Periodical Reports Electron Spin Resonance Series*, B.C. Gilbert, M.J. Davies and D.M. Murphy (eds), Royal Society of Chemistry, Cambridge, 2004, **19**, 374.
3. G. Zoppellaro, V. Enkelmann, A. Geies and M. Baumgarten, *Org. Lett*., 2004, **6**, 4929.
4. K. Komaguchi, T. Iida, Y. Goh, J. Oshita, A. Kanui and M. Shiotani, *Chem. Phys. Lett*., 2004, **387**, 327.
5. R. Ziessel, C. Stroh, H. Heise, F.H. Köhler, P. Yurek, N. Claiser, M. Souhassou and C. Lecomte, *J. Am. Chem. Soc*., 2004, **126**, 12604.
6. C. Stroh, M. Mayor and C. von Hanisch, P Turek, *Chem. Commun*., 2004, 2050.
7. K. Maekawa, D. Shiomi, T. Ise, K. Sato and T. Takui, *J. Phys. Chem. B*, 2005, **109**, 3303.
8. L. Catala, J. Le Moigne, N. Gruber, J.J. Novoa, P. Rabu, E. Belorizky and P. Turek, *Chem. Eur. J*., 2005, **11**, 2440.
9. C. Rancurel, H. Heise, F.H. Köhler, U. Schatzschneider, E. Rentschler, J. Vidal-Gancedo, J. Veciana and J.-P. Sutter, *J. Phys. Chem. A*, 2004, **108**, 5903.
10. O.B. Borobia, P. Gionneau, H. Heise, F.H. Köhler, L. Ducasse, J. Vidal-Gancedo, J. Veciana, S. Golhen, L. Ouahab and J.-P. Sutter, *Chem. Eur. J*., 2005, **11**, 128.
11. G.A. Carriedo, F.J. Garcia Alonso, P.G. Elipe, E. Brillas, A. Labarta and L. Juliá, *J. Org. Chem*., 2004, **69**, 99.
12. A. Rajca, K. Shiraishi, M. Vale, H. Han and S. Rajca, *J. Am. Chem. Soc*., 2005, **127**, 9014.
13. C. Elschenbroich, J. Plackmeyer, M. Nowotny, K. Harms, J. Pebler and O. Burghaus, *Inorg. Chem*., 2005, **44**, 955.
14. C. Elschenbroich, J. Plackmeyer, M. Nowotny, A. Behrendt, K. Harms, J. Pebler and O. Burghaus, *Chem. Eur. J*., 2005, **11**, 7427.
15. C. Elschenbroich, O. Schiemann, O. Burghaus and K. Harms, *Chem. Commun*., 2005, 2149.
16. C. Elschenbroich, M. Wünsch, A. Behrend, B. Metz, B. Neumüller and K. Harms, *Organometallics*, 2005, **24**, 5509.
17. W.W.H. Wong, J. Cookson, E.A.L. Evans, E.J.L. McInnes, J. Wolowska, J.P. Maher, P. Bishop and P.D. Beer, *Chem. Commun*., 2005, 2214.
18. A.D. Bond, S. Derossi, C.J. Harding, E.J.L. McInnes, V. McKee, C.J. McKenzie, J. Nelson and J. Wolowska, *Dalton Trans*., 2005, 2403.
19. J. Yano, K. Sauer, J.-J. Girerd and V.K. Yachandra, *J. Am. Chem. Soc*., 2004, **126**, 7486.

20. X. Liu, M.P. de Miranda, E.J.L. McInnes, C.A. Kilner and M.A. Halcrow, *Dalton Trans.*, 2004, 59.
21. J. Yoon, L.M. Mirica, T.D.P. Stack and E.I. Solomon, *J. Am. Chem. Soc.*, 2004, **126**, 12586.
22. J. Yoon and E.I. Solomon, *Inorg. Chem.*, 2005, **44**, 8076.
23. I. Gautier-Luneau, D. Phanon, C. Duboc, D. Luneau and J.-P. Pierre, *Dalton Trans.*, 2005, 3795.
24. O. Kahn, *Chem. Phys. Lett.*, 1997, **265**, 109.
25. T. Glaser, M. Heidmeier, S. Grimme and E. Bill, *Inorg. Chem.*, 2004, **43**, 5192.
26. S. Nellutla, J. Van Tol, N.S. Dalal, L.-H. Bi, U. Kortz, B. Keita, L. Nadjo, G.A. Khitrov and A.G. Marshall, *Inorg. Chem.*, 2005, **44**, 9795.
27. X. Liu, J.A. McAllister, M.P. de Miranda, E.J.L. McInnes, C.A. Kilner and M.A. Halcrow, *Chem. Eur. J.*, 2004, **10**, 1827.
28. B. Pilawa, R. Boffinger, I. Keilhauer, R. Leppin, I. Odenwald, W. Wendl, C. Berthier and M. Horvatić, *Phys. Rev. B*, 2005, **71**, 184419.
29. O. Cador, D. Gatteschi, R. Sessoli, A.-L. Barra, G.A. Timco and R.E.P. Winpenny, *J. Magn. Magn. Mat.*, 2005, **290–291**, 55.
30. S. Sharmin, A. Ardavan, S.J. Blundell, A.I. Coledea, E.J.L. McInnes and D. Low, *Appl. Phys. Lett.*, 2005, **86**, 032507.
31. H. Oshio, M. Nihei, A. Yoshida, H. Nohiri, M. Nakano, A. Yamaguchi, Y. Karaki and H. Ishimoto, *Chem. Eur. J.*, 2005, **11**, 843.
32. C. Kirman, J. Lawrence, S. Hill, E.-C. Yang and D.N. Hendrickson, *J. Appl. Phys.*, 2005, **97**, 10M501.
33. D.N. Hendrickson, E.-C. Yang, R.M. Isidro, C. Kirman, J. Lawrence, R.S. Edwards, S. Hill, A. Yamaguchi, H. Ishimoto, W. Wernsdorfer, C. Ramsey, N. Dalal and M.M. Olmstead, *Polyhedron*, 2005, **24**, 2280.
34. A. Cornia, A.C. Fabretti, P. Garrisi, C. Mortaló, D. Bonacchi, D. Gatteschi, R. Sessoli, L. Sorace, W. Wernsdorfer and A.-L. Barra, *Angew. Chem. Int. Ed.*, 2004, **43**, 1136.
35. A. Cornia, A.C. Fabretti, P. Garrisi, C. Mortaló, D. Bonacchi, R. Sessoli, L. Sorace, A.-L. Barra and W. Wernsdorfer, *J. Magn. Magn. Mat.*, 2004, **272–276**, e749.
36. N. Aliaga-Alcalde, R.S. Edwards, S.O. Hill, W. Wernsdorfer, K. Folting and G. Christou, *J. Am. Chem. Soc.*, 2004, **126**, 12503.
37. J. van Slageren, S. Vontragool, B. Gorshunov, A.A. Mukhin, N. Karl, J. Krzystek, J. Telser, A. Müller, C. Sangregorio, D. Gateschi and M. Dressel, *Phys. Chem. Chem. Phys.*, 2003, **5**, 3837.
38. S. Piligkos, G. Rajaraman, M. Soler, N. Kirchner, J. Van Slageren, R. Bircher, S. Parsons, H.-U. Güdel, J. Kortus, W. Wernsdorfer, G. Chrsitou and E.K. Brechin, *J. Am. Chem. Soc.*, 2005, **127**, 5572.
39. N. Kirchner, J. van Slageren, E.K. Brechin and M. Dressel, *Polyhedron*, 2005, **24**, 2400.
40. S. Vongtragool, B. Gorshunov, J. van Slageren, M. Dressel and A.A. Mukhin, *J. Magn. Magn. Mat.*, 2004, **272–276**, e769.
41. S. Vongtragool, A. Mukhin, B. Gorshunov and M. Dressel, *Phys. Rev. B*, 2004, **69**, 104410.
42. A. Cornia, R. Sessoli, L. Sorace, D. Gatteschi, A.-L. Barra and C. Daiguebonne, *Phys. Rev. Lett.*, 2002, **89**, 257201.
43. S. Takahashi, R.S. Edwards, J.M. North, S. Hill and N.S. Dalal, *Phys. Rev. B*, 2004, **70**, 094429.

44. S. Hill, N. Anderson, A. Wilson, S. Takahashi, K. Petukhov, N.E. Chakov, M. Murugesu, J.M. North, E. del Barco, A.D. Kent, N.S. Dalal and G. Christou, *Polyhedron*, 2005, **24**, 2284.
45. S. Hill, N. Anderson, A. Wilson, S. Takahashi, N.E. Chakov, M. Murugesu, J.M. North, N.S. Dalal and G. Christou, *J. Appl. Phys.*, 2005, **97**, 10M510.
46. K. Petukhov, S. Hill, N.E. Chakov, K.A. Abboud and G. Christou, *Phys. Rev. B*, 2004, **70**, 054426.
47. E.M. Rumberger, E. Del Barco, J. Lawrence, S. Hill, A.D. Kent, L.N. Zakharov, A.L. Rheingold and D.N. Hendrickson, *Polyhedron*, 2005, 2557.
48. H. Hachisuka, K. Awaga, T. Yokoyama, T. Kubo, T. Goto and H. Nojiri, *Phys. Rev. B*, 2004, **70**, 104427.
49. S. Piligkos, D. Collison, V.S. Oganesyan, G. Rajaraman, G.A. Timco, A.J. Thomson, R.E.P. Winpenny and E.J.L. McInnes, *Phys. Rev. B*, 2004, **69**, 134424.
50. K. Petukhov, W. Wernsdorfer, A.-L. Barra and V. Mosser, *Phys. Rev. B*, 2005, **72**, 052401.
51. B. Cage, S.E. Russek, D. Zipse and N.S. Dalal, *J. Appl. Phys.*, 2005, **97**, 10M507.
52. B. Cage, S.E. Russek, D. Zipse, J.M. North and N.S. Dalal, *Appl. Phys. Lett.*, 2005, **87**, 082501.
53. K. Chlopek, E. Bill, T. Weyhermüller and K. Wieghardt, *Inorg. Chem.*, 2005, **44**, 7087.
54. K. Ray, E. Bill, T. Weyhermüller and K. Wieghardt, *J. Am. Chem. Soc.*, 2005, **127**, 5641.
55. F. Thomas, O. Jarjayes, C. Duboc, C. Philouze, E. Saint-Aman and J.-L. Pierre, *Dalton Trans.*, 2004, 2662.
56. M.L. Kirk, D.A. Shultz and E.C. Depperman, *Polyhedron*, 2005, **24**, 2880.
57. D.S. Marlin, E. Bill, T. Weyhermüller, E. Bothe and K. Wieghardt, *J. Am. Chem. Soc.*, 2005, **127**, 6095.
58. Y. Yukawa, G. Aromi, S. Igarashi, J. Ribas, S.A. Zvyagin and J. Krzystek, *Angew. Chem. Int. Ed.*, 2005, **44**, 1997.
59. C. Elsaesser, M. Brecht and R. Bittl, *Biochem. Soc.*, 2004, **33**, 15.
60. T. Maly, F. MacMillan, K. Zwicker, N. Kashani-Poor, U. Brandt and T.F. Prisner, *Biochemistry*, 2004, **43**, 3969.
61. P.C. Dos Santos, R.Y. Igarashi, H.-I. Lee, B.M. Hoffman, L.C. Seefeldt and D.R. Dean, *Acc. Chem. Res.*, 2005, **38**, 208.
62. T.-C. Yang, N.K. Maeser, M. Laryukhin, H.-I. Lee, D.R. Dean, L.C. Seefeldt and B.M. Hoffman, *J. Amer. Chem. Soc.*, 2005, **127**, 12804.
63. H.-I. Lee, R.Y. Igarashi, M. Laryukhin, P.E. Doan, P.C. Dos Santos, D.R. Dean, L.C. Seefeldt and B.M. Hoffman, *J. Amer. Chem. Soc.*, 2004, **126**, 9563.
64. B.M. Barney, T.-C. Yang, R.Y. Igarashi, P.C. Dos Santos, M. Laryukhin, H.-I. Lee, B.M. Hoffman, D.R. Dean and L.C. Seefeldt, *J. Amer. Chem. Soc.*, 2005, **127**, 14960.
65. B.M. Barney, M. Laryukhin, R.Y. Igarashi, H.-I. Lee, P.C. Dos Santos, T.-C. Yang, B.M. Hoffman, D.R. Dean and L.C. Seefeldt, *Biochemistry*, 2005, **44**, 8030.
66. R.Y. Igarashi, M. Laryukhin, P.C. Dos Santos, H.-I. Lee, D.R. Dean and L.C. Seefeldt, and B.M. Hoffman, *J. Amer. Chem. Soc.*, 2005, **127**, 6231.
67. K. Fisher and W.E. Newton, *Biochim. Biophys. Acta*, 2005, **1750**, 154.
68. Z. Maskos, K. Fisher, M. Sørlie, W.E. Newton and B.J. Hales, *J. Biol. Inorg. Chem.*, 2005, **10**, 394.
69. Y. Hu, M.C. Corbett, A.W. Fay, J.A. Webber, B. Hedman and K.O. Hodgson, *Proc. Nat. Acad. Sci.*, 2005, **102**, 13825.

70. J. Petersen, C. Gessner, K. Fisher, C.J. Mitchell, D.J. Lowe and W. Lubitz, *Biochem. J.*, 2005, **391**, 527.
71. I. Galli, G. Musci and M.C. Bonaccorsi di Patti, *J. Biol. Inorg. Chem.*, 2004 **9**, 90.
72. L. Quintanar, C. Stoj, T.-P. Wang, D.J. Kosman and E.I. Solomon, *Biochemistry*, 2005, **44**, 6081.
73. L. Quintanar, J. Yoon, C.P. Aznar, A.E. Palmer, K.K. Andersson, R.D. Britt and E.I. Solomon, *J. Amer. Chem. Soc.*, 2005, **127**, 13832.
74. M.R. Cheesman, V.S. Oganesyan, N.J. Watmough, C.S. Butler and A.J. Thomson, *J. Amer. Chem. Soc.*, 2004, **126**, 4157.
75. Y. Matsuda, T. Uchida, H. Hori, T. Kitagawa and H. Arata, *Biochim. Biophys. Acta*, 2004, **1656**, 37.
76. C. Teutloff, K.-O. Schäfer, S. Sinnecker, V. Barynin, R. Bittl, K. Weighardt, F. Lendzian and W. Lubitz, *Magn. Reson. Chem.*, 2005, **43**, S51.
77. C.R. Samples, T. Howard, F.M. Raushel and V.J. DeRose, *Biochemistry*, 2005, **44**, 11005.
78. B. Epel, K.-O. Schäfer, A. Quentmeier, C. Friedrich and W. Lubitz, *J. Biol. Inorg. Chem.*, 2005, **10**, 636.
79. C. More, M. Asso, G. Roger, B. Guigliarelli, J. Caldeira, J. Moura and P. Betrand, *Biochemistry*, 2005, **44**, 11628.
80. M. Uhlmann and T. Friedrich, *Biochemistry*, 2005, **44**, 1653.
81. M. Verkhovskaya, L. Sinegina, M. Wikström and M. Verkhovsky, *Biochim. Biophys. Acta*, 2004, **1658**, 141.
82. J.W. Cooley, A.G. Roberts, M.K. Bowman, D.M. Kramer and F. Daldal, *Biochemistry*, 2004, **43**, 2217.
83. J. Tatur and W.R. Hagen, *FEBS Lett.*, 2005, **579**, 4729.
84. G.N.L. Jameson, M.M. Cosper, H.L. Hernández, M.K. Johnson and B.H. Huynh, *Biochemistry*, 2004, **43**, 2022.
85. C.J. Walsby, D. Ortillo, J. Yang, M.R. Nnyepi, W.E. Broderick, B.M. Hoffman and J.B. Broderick, *Inorg. Chem.*, 2005, **44**, 727.
86. E. Nakamura-Ogiso, T. Yano, T. Yagi and T. Ohnishi, *J. Biol. Chem.*, 2005, **280**, 301.
87. R.M. Cicchillo, K.-H. Lee, C. Baleanu-Gogonea, N.M. Nesbitt, C. Krebs and S.J. Booker, *Biochemistry*, 2004, **43**, 11770.
88. L. Sinegina, M. Wikström, M.I. Verkhovsky and M.L. Verkhovskaya, *Biochemistry*, 2005, **44**, 8500.
89. T. Shirakawa, Y. Takahashi, K. Wada, J. Hirota, T. Takao, D. Ohmori and K. Fukuyama, *Biochemistry*, 2005, **44**, 12402.
90. A.H. Priem, A.A.K. Klaassen, E.J. Reijerse, T.E. Meyer, C. Luchinat, F. Capozzi, W.R. Dunham and W.R. Hagen, *J. Biol. Inorg. Chem.*, 2005, **10**, 417.
91. L. Forzi, J. Koch, A.M. Guss, C.G. Radosevich, W.W. Metcalf and R. Hedderich, *FEBS J.*, 2005, **272**, 4741.
92. A.K. Boal, E. Yavin, O.A. Lukianova, V.L. O'Shea, S.S. David and J.K. Barton, *Biochemistry*, 2005, **44**, 8397.
93. R.M. Cicchillo, M.A. Baker, E.J. Schnitzer, E.B. Newman, C. Krebs and S.J. Booker, *J. Biol. Chem.*, 2004, **279**, 32418.
94. V.W.T. Cheng, R.A. Rothery, M.G. Bertero, N.C.J. Strynadka and J.H. Weiner, *Biochemistry*, 2005, **44**, 8068.
95. R.A. Rothery, M.G. Bertero, R. Cammack, M. Palak, F. Blasco, N.C.J. Strynadka and J.H. Weiner, *Biochemistry*, 2004, **43**, 5324.

96. C.D. Brondino, M.C.G. Passeggi, J. Caldeira, M.J. Almendra, M.J. Feio, J.J.G. Moura and I. Moura, *J. Biol. Inorg. Chem.*, 2004, **9**, 145.
97. M. Bennati, N. Weiden, K.-P. Dinse and R. Hedderich, *J. Amer. Chem. Soc.*, 2004, **126**, 8378.
98. E.M. Walters and M.K. Johnson, *Photosynth. Res.*, 2004, **79**, 249.
99. P. Hänzelmann, H.L. Hernández, C. Menzel, R. García-Serres, B.H. Huynh, M.K. Johnson, R.R. Mendel and H. Schindelin, *J. Biol. Chem.*, 2004, **279**, 34721.
100. M. Heinnickel, G. Shen, R. Agalarov and J.H. Golbeck, *Biochemistry*, 2005, **44**, 9950.
101. R.D. Britt, K.A. Campbell, J.M. Peloquin, M.L. Gilchrist, C.P. Aznar, M.M. Dicus, J. Robblee and J. Messinger, *Biochim. Biophys. Acta*, 2004, **1655**, 158.
102. M.-F. Charlot, A. Boussac and G. Blondin, *Biochim. Biophys. Acta*, 2005, **1708**, 120.
103. H. Yu, P. Aznar, X. Xu and R.D. Britt, *Biochemistry*, 2005, **44**, 12022.
104. W. Gregor, R.M. Cinco, H. Yu, V.K. Yachandra and R.D. Britt, *Biochemistry*, 2005, **44**, 8817.
105. S.H. Kim, W. Gregor, J.M. Peloquin, M. Brynda and R.D. Britt, *J. Amer. Chem. Soc.*, 2004, **126**, 7228.
106. L.V. Kulik, W. Lubitz and J. Messinger, *Biochemistry*, 2005, **44**, 9368.
107. L.V. Kulik, B. Epel, W. Lubitz and J. Messinger, *J. Amer. Chem. Soc.*, 2005, **127**, 2392.
108. F. Mamedov, P.J. Smith, S. Styring and R.J. Pace, *Phys. Chem. Chem. Phys.*, 2004, **6**, 4890.
109. D. Koulougliotis, C. Teutloff, Y. Sanakis, W. Lubitz and V. Petrouleas, *Phys. Chem. Chem. Phys.*, 2004, **6**, 4859.
110. L. Kulik, B. Epel, J. Messinger and W. Lubitz, *Photosynth. Res.*, 2005, **84**, 347.
111. K.A. Århling, M.C.W. Evans, J.H.A. Nugent and R.J. Pace, *Biochim. Biophys. Acta*, 2004, **1656**, 66.
112. M.C.W. Evans, J.H.A. Nugent, R.J. Ball, I. Muhiuddin and R.J. Pace, *Biochemistry*, 2004, **43**, 989.
113. Y. Kimura, N. Mizusawa, A. Ishii, S. Nakazawa and T.-a. Ono, *J. Biol. Chem.*, 2005, **280**, 37895.
114. M. van Gastel, C. Fichtner, F. Neese and W. Lubitz, *Biochem. Soc. Trans.*, 2005, **33**, 7.
115. S. Foerster, M. van Gastel, M. Brecht and W. Lubitz, *J. Biol. Inorg. Chem.*, 2005, **10**, 51.
116. J. Seravalli, Y. Xiao, W. Gu, S.P. Cramer, W.E. Antholine, V. Krymov, G.J. Gerfen and S.W. Ragsdale, *Biochemistry*, 2004, **43**, 3944.
117. J.M. Canfield and K. Warncke, *J. Phys. Chem. B*, 2005, **109**, 3053.